# FIRSTHAND LEARNING OF THE CIRCULATION AND STRATIFICATION OFF SABRINA COAST, ANTARCTICA

A Thesis

by

NATALIE JANE ZIELINSKI

Submitted to the Office of Graduate and Professional Studies of
Texas A&M University
in partial fulfillment of the requirements for the degree of

MASTER OF SCIENCE

| | |
|---|---|
| Chair of Committee, | Alejandro H. Orsi |
| Committee Members, | Achim Stössel |
| | Gerald R. North |
| Head of Department, | Debbie Thomas |

August 2016

Major Subject: Oceanography

## ABSTRACT

Air-sea-ice interaction observed within the Sabrina Basin, East Antarctica are likely widespread along the Antarctica margins, therefore this study is relevant to explaining and predicting current mass loss trends in other Antarctic ice shelves and glaciers. Water mass structure, mixing history and flow patterns over the continental shelf off Sabrina Coast (115 °E - 122 °E) are described using the first observations made during the multi-disciplinary U.S. cruise of 2014 and the follow up Australian cruise of 2015 and based on dynamic topographies at selected levels, property distributions on specific isopycnals and levels.

Two large cyclones are inferred over the shelf, an elongated one connecting slope waters to the eastern end of the escarpment, and a zonally-oriented cell connecting the westward boundary current along the northern escarpment to the interior of the Dalton Basin. Unlike the available Modified Circumpolar Deep Water near the shelf break, the lighter Thermocline Water is able to enter the shelf over the Dalton Basin sill (~450 m), progressively deepening within the bottom layer temperature maximum of an eastern boundary current found against the western flank of the Dalton Plateau (450 m – 550 m). Near the southern end of the Plateau its densest remnant branches westward and further sinks to depths greater than 550 m supplying the warmest bottom layer within the southern limb of the Dalton Basin cyclone. Relatively lighter Thermocline Water ($\gamma^n$ = 27.90 kg $m^3$) lying at about 150 m near the shelf break extends to over the escarpment at 450 m, and supplies multiple trenches connected to Moscow University Ice Shelf with source water warmer than -1.7 °C at 560 m available for basal melt. Directly above this

inflow, a prominent Meltwater-bearing outflow is observed at the Central Trench of this Ice Shelf over a 300-m thick layer with water colder than -1.8 °C and fresher than 34.22 ($\gamma^n$ < 27.90 kg $m^3$), whose downstream influence throughout the Sabrina Basin cyclonic flow is evident by a thickened thermostad layer and much deeper interior thermocline than over the eastern shelf. Ventilation of the oceanic Thermocline Water takes place along a tight anticyclonic loop west of the Dalton Iceberg Tongue. Here, a relatively warm ($\theta$ > -1.83 °C) and saline (S > 34.30) southeastward inflow at 200 m ($\gamma^n$ > 27.90 kg $m^3$) impinges onto the northern Tongue, and emerges off its tip as a fresh (S < 34.22) and lighter ($\gamma^n$ < 27.80 kg $m^3$) plume injected northwestward into the Antarctic Slope Current.

## DEDICATION

This work is dedicated to my parents, Bob and Jane Zielinski, who have always supported my passion for the ocean. For without their continuous love, verbal encouragement, and financial assistance this work would not have been possible. I owe all that I am as a woman and a scientist to them and will be forever grateful.

“For whatever we lose, It’s always our self we find in the sea.” –e.e. Cummings

## ACKNOWLEDGEMENTS

I owe the completion of this research to many people. I would like to acknowledge NSF support from a grant to Dr. Orsi that made my first, and hopefully not last, participation on an oceanographic cruise to Antarctica possible.

I want to thank my academic advisor, Dr. Alejandro H. Orsi, for his limitless support and guidance in the development of this research, and for giving me the confidence I needed to start asking my own questions. I want to thank my committee members Dr. Stössel and Dr. North for their patience during this processes.

I also want to thank the graduate students of the Department of Oceanography for reminding me to take time for myself, for countless hours of laughter, and being available for venting sessions. Specifically, I thank Claire McKinley for listening and always providing motivation. Thank you Andrea Kealoha for putting my worries at ease and for my newfound addiction to yoga, which has maintained my mental and physical health through this journey. Thanks Cody Webb for putting up with my singing as we worked in our shared office space and for always being available to help decode limitless mysteries of MATLAB.

## NOMENCLATURE

| | |
|---|---|
| AABW | Antarctic Bottom Water |
| AASW | Antarctic Surface Water |
| ACC | Antarctic Circumpolar Current |
| ADCP | Acoustic Doppler Current Profiler |
| ASF | Antarctic Slope Front |
| CDW | Circumpolar Deep Water |
| CTD | Conductivity, Temperature, Depth |
| DB | Dalton Bank |
| DD | Dalton Depression |
| DIT | Dalton Iceberg Tongue |
| DP | Dalton Polynya |
| DPL | Dalton Plateau |
| EAIS | East Antarctic Ice Sheet |
| MCDW | Modified Circumpolar Deep Water |
| MP | Mertz Polynya |
| MTW | Modified Thermocline Water |
| MUIS | Moscow University Ice Shelf |
| MW | Meltwater |
| PIG | Pine Island Glacier |
| SW | Shelf Water |
| TG | Totten Glacier |

| | |
|---|---|
| TW | Thermocline Water |
| uCTD | Underway Conductivity, Temperature, Depth |
| WAIS | West Antarctic Ice Sheet |

## TABLE OF CONTENTS

## LIST OF FIGURES

## LIST OF TABLES

# 1. INTRODUCTION

## 1.1. Changing Antarctic Cryosphere

The largest volume of fresh water on Earth is stored in two continental ice sheets on Antarctica, the West Antarctic Ice Sheet (WAIS) and the East Antarctic Ice Sheet (EAIS), equivalent to a potential global sea level rise (SLR) of 3.3 m and 47 m [*IPCC*, 2013]. The interaction of the ocean with the edges of these ice sheets is of special interest because, through basal melt, the effects impact ice sheet stability and SLR. A continental ice sheet is considered stable if it gains as much mass in the interior, through precipitation, as it loses around the edges, through basal melt and calving. Ice streams flow downslope from the interior toward the ocean, supplying mass to floating glaciers and ice shelves. The latter provide enough backpressure, from fringe buttressing, to maintain continental ice discharge at a steady state; otherwise it could potentially accelerate SLR [*Dupont and Alley*, 2005; *Feldmann and Levermann*, 2015].

Increased heat content of the Earth Climate System over the past few decades has lead to warming of the upper ocean [*Abraham et al.,* 2013; *IPCC*, 2013]. The Southern Ocean has warmed at a decadal rate more than double the average global rate [*Gille*, 2002; *IPCC*, 2013]. Potential consequences of this additional available oceanic heat are the recent fall of ice steams surface and increase in basal melt of ice shelves at some Antarctic margins [*Davis et al.,* 2005; *IPCC*, 2013; *Liu et al.,* 2015; *Prichard et al.,* 2012; *Shepherd et al.,* 2004; *Rignot,* 2013].

The WAIS shows some of the highest estimated ice stream velocities, and rates of basal melt and elevation loss in Antarctica [*Davis et al.,* 2005; *Liu et al.,* 2015; *Jacobs*

*et al.,* 2011; *Rignot,* 2013; *Rignot and Thomas,* 2002]. Evidence of how rapidly WAIS may adjust to future atmospheric and oceanic temperature changes was observed during the week-long collapse of the Larsen B Ice Shelf (60°W) in 2002, in spite of the available Circumpolar Deep Water (CDW) being the coldest (~θ = 0.5 °C; Figure 1a) around Antarctica [*Whitworth et al.,* 1998]. The contribution to SLR was immediate as the result of enhanced discharge from local ice streams [*Scambos et al.,* 2004]. CDW inflows to the southeast Pacific shelf are the warmest (θ = 2 °C). A relatively thick bottom layer with θ > 1 °C extends uninterrupted to the entrance of Pine Island Glacier (PIG) sub-ice cavity [*Rignot and Thomas,* 2002, *Jacobs et al*., 2011]. In the Bellingshausen-Amundsen Sea region (130°W – 70°W), the poleward oceanic heat transport controls the overall stability of WAIS [*Rignot*, 2013].

One of the most climate-relevant areas of the EAIS is the Aurora Subglacial Basin, because it includes ice streams feeding the Totten Glacier (TG) and Moscow University Ice Shelf (MUIS), whose combined SLR potential amounts to 6.9 m. These ice streams show similar changes in velocity, elevation loss, and melt rates to those in the Amundsen Sea [*Davis et al.,* 2005; *Khazendar et al.,* 2013; *Liu et al*., 2015; *Rignot and Thomas,* 2002; *Wingham et al.,* 2009], suggesting increased accessibility of oceanic heat to the sub-ice cavities found off Sabrina Coast (115 °E – 122 °E; Figure 1). Pritchard et al., [2012] shows the warmest ocean bottom temperatures with access to EAIS near TG/MUIS, apparently directly inshore of a measured bottom water inflow with θ =1.2 °C near the shelf break [*Bindoff et al.*, 2011]. However, the lack of direct observations over this margin prevents any attempt to explain the regional air-sea-ice

responses to ongoing climate change. In fact, the first-time shipboard observations in this area were obtained during the austral summers of 2014 and 2015. Therefore, the newly available data sets warrant initial studies of ocean circulation and stratification over the continental shelf off Sabrina Coast, and the inferred interactions of local water masses with the underlying bottom topography and surrounding Dalton Iceberg Tongue (DIT), MUIS and TG.

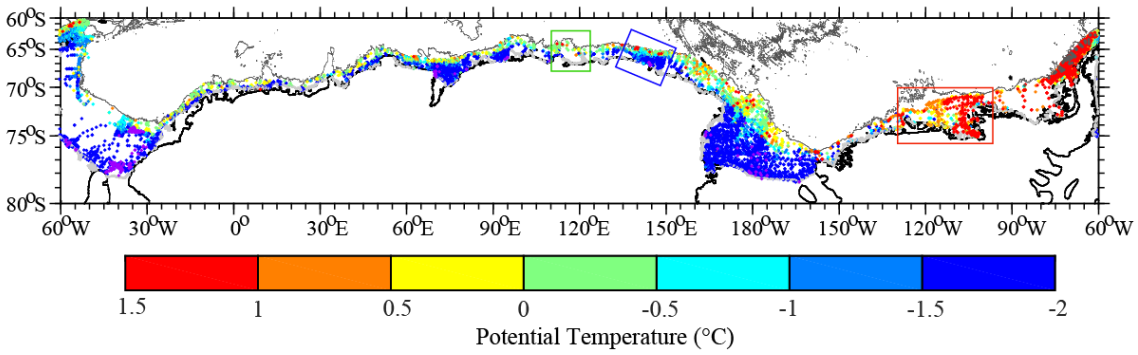


(a)

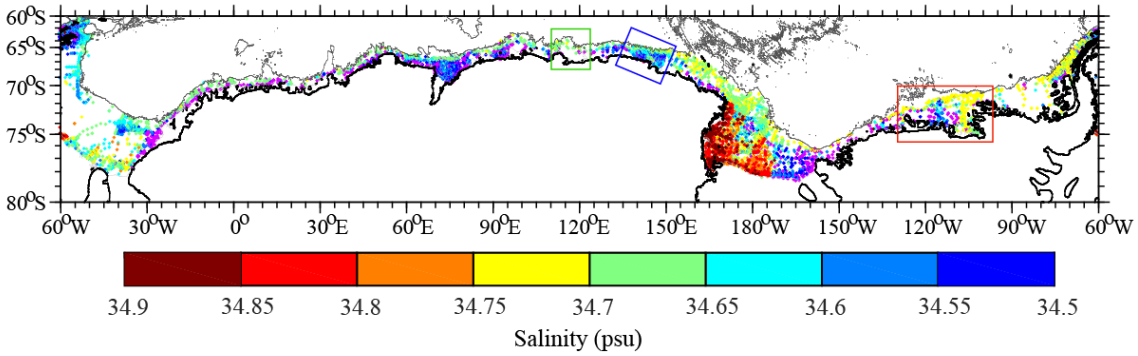


(b)

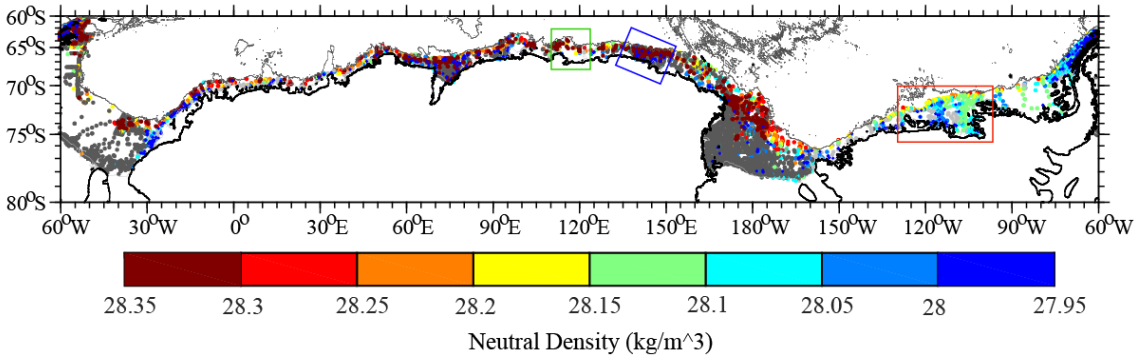


(c)

Figure 1. Map of bottom (a) potential temperature, (b) salinity, and (c) neutral density for all stations inshore of the 3000-m isobath shown by the thin gray line. Red, blue and green boxes centered at 110°W, 140°E and 120°E include stations in the Amundsen Sea, Mertz Basin and Sabrina Basin.

## 2. STRATIFICATION OF ANTARCTIC MARGINS

### 2.1. Cross-slope Exchange

The most voluminous water mass in the Southern Ocean is the CDW carried eastward around Antarctica by the Antarctic Circumpolar Current (ACC) [*Worthington*, 1981]. As the southern boundary of the ACC extends over the upper slope in the Bellingshausen Sea and Drake Passage (100°W – 60 °W, Figure 1a-c), extremely warm, saline and oxygen-poor CDW floods the local shelves. Where the path of the ACC is far from the continental margins, CDW drawn from the ACC circulates cyclonically within large subpolar gyres in the Weddell-Enderby Abyssal Plain, the Australian-Antarctic Basin, and the Amundsen Abyssal Plain. Here CDW is clearly identified by relatively high temperatures (below a θ-max) at subsurface to intermediate levels, between the much colder Antarctic Surface Water (AASW) above, which includes the thin horizontal Thermocline Water (TW) layer between the θ-min and θ-max, and the Antarctic Bottom Water (AABW) below ($\gamma^n > 28.27$ kg $m^3$). Poleward-flowing eastern limbs (30°E - 40 °E, 120°E -130 °E, 140°W – 150°W, Figure 1a) bring relatively warmer CDW to the shelf sectors immediately downstream. Except for the Bellingshausen and southern Drake Passage sector, the diving of the oceanic thermocline at the upper continental slope is indicated by a strong subsurface (200 m -600 m) property gradients (water depths < 800 m) known as Antarctic Slope Front (ASF) [*Jacobs*, 1991*; Schroder and Fahrbach*, 1999; *Whitworth* et al., 1998; *Bindoff* et al., 2001]. Here CDW mixes with a thickened layer of AASW inshore, attenuating the extreme characteristics of local TW and CDW available to continue poleward across the shelf, as Modified TW and CDW

(MTW and MCDW). Thus the upper (lower) limit of local CDW (TW) available near the slope varies regionally around Antarctica; they are defined by the neutral density ($\gamma^n$) surfaces of the θ-max (θ-min) observed at the slope's 3000-m isobath [*Whitworth et al.*, 1998].

### 2.1.1. Dominant Oceanic Input

The Amundsen Sea (120°W - 100 °W) shows some of the most prominent poleward extent and influence of CDW. Local CDW (TW) at the lower portion of the slope is warmer than 1.9 °C (θ-max at $\gamma^n$ = 27.95 kg $m^3$, green station in Figure 2a-b) (colder than -1.2°C at $\gamma^n$ < 27.60 kg $m^3$), but it cools (freshens) to 1.2 °C as it overrides the shelf break sills. The oceanic thermocline is slightly tilted across the shelf break, i.e. poleward from about 150 m to 350 m, which facilitates oceanic inputs to extend farther inshore within a relatively thick bottom θ-max layer with θ > 1 °C (Figure 2c) [*Jacobs et al.,* 2011; *Jacobs and Hellmer,* 1996; *Jenkins et al.,* 2010; *Payne et al.,* 2007; *Schodlok et al.,* 2012] (Figure 1a-c). After minimum cross-shelf cooling (θ = 0.5 °C), freshening (S = 0.05) and deepening (depth = 250 m) [*Jacobs et al.,* 2011], the source bottom water to basal melt continuing below the PIG is about 3.5 °C warmer than the in situ freezing point.

At intermediate depths (200 m – 400 m) at the ice edge a portion of an outflowing buoyancy plume incorporates local Meltwater (MW) [*Arrigo et al., 2012*; *Mankoff et al.,* 2012; *Yager et al.,* 2012]. In TS space the signal of attenuating MW is detected about 300 km north of the ice front, as indicated by the straight portion of abnormally warm local TW (MTW).

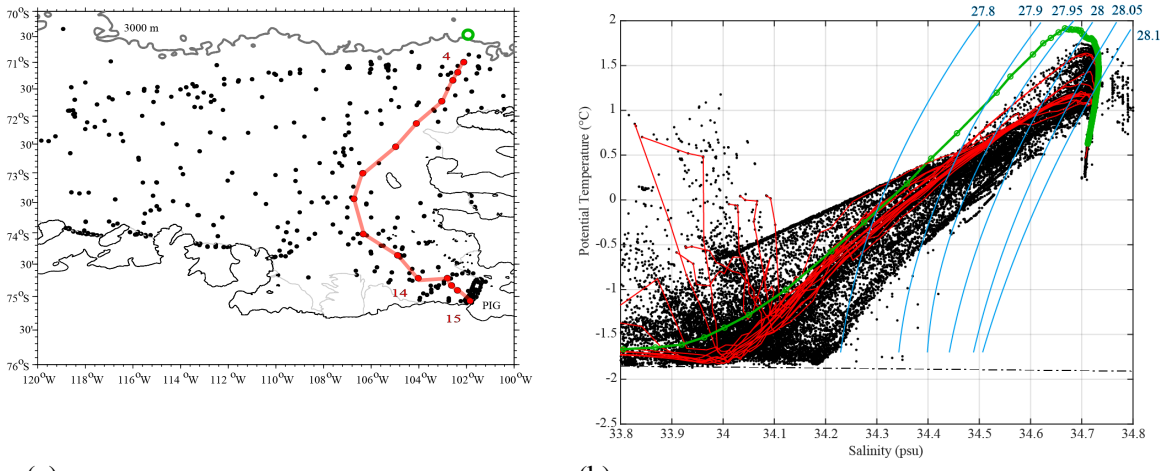


(a) (b)

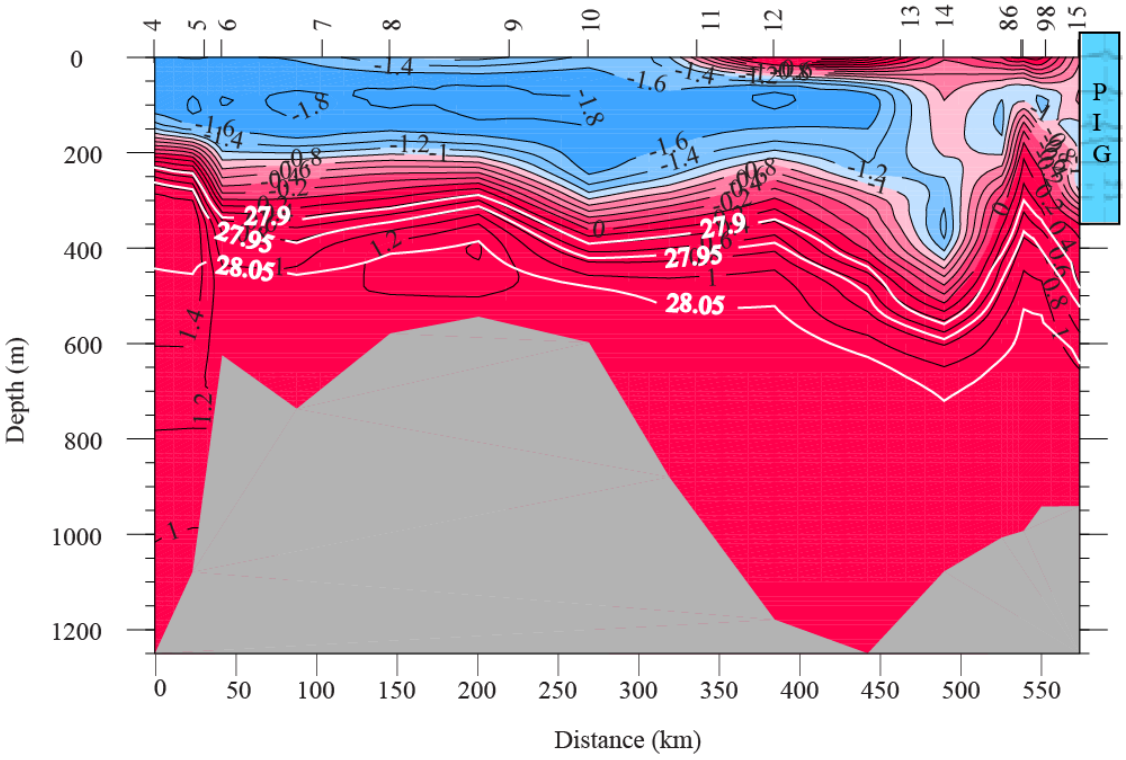


(c)

Figure 2. (a) Location of stations over the Amundsen Sea margins; (b) scatter plot of their potential temperature vs. salinity, with thin cyan lines being the traces of selected neutral density surfaces; and (c) vertical distribution of potential temperature for the red stations shown in (a). Thick white contours are of selected neutral density surfaces. The green station shown in (a-b) characterizes the warmest available CDW, whereas red stations depict the cross-shelf water mass structure.

### 2.1.2. Constrained Access by Marginal Waters

Intrusion of CDW to most other sectors is often limited by the production rate and circulation pattern of lighter and denser waters found over the shelf [*Whitworth et al.,* 1998]. Near other large shelf embayments (Ross, Mertz, Prydz, and Weddell Seas) and along the narrower continental shelves in between, poleward intrusion of TW and MCDW are dynamically regulated by the Antarctic Slope Current associated to a deep expression of the ASF, as it interacts with the local sills near the self break.

Inflow to the shelf off Sabrina Coast has been inferred from interpretation [*Williams et al.*, 2011] of limited observations at 120 °E from the 1996 BROKE survey (red stations in Figure 3a-b). The warmest CDW (TW) available at the deeper slope is warmer (colder) than 1.4 °C with a θ-max at $\gamma^n$ = 28.08 kg m$^3$ (-1.8°C with a θ-min at $\gamma^n$ < 27.90 kg m$^3$) (green station), whereas the MCDW found at the shelf break (Sta. 83) just south of the ASF (Stas. 84-89) is colder than 0.7°C. Unlike in the Amundsen Sea, there is a prominent deep-reaching (150 m - 450 m) local expression of the ASF effectively blocking the poleward reach of local MCDW to the floating ice shelves and glaciers with SLR potential (Figure 3c). The slightly tilted thermocline at the shelf break of the Amundsen Sea clears the sill by about 250 m, whereas at the Sabrina Basin (120°E) it dives about 300 m into sill over a similar distance (20 km).

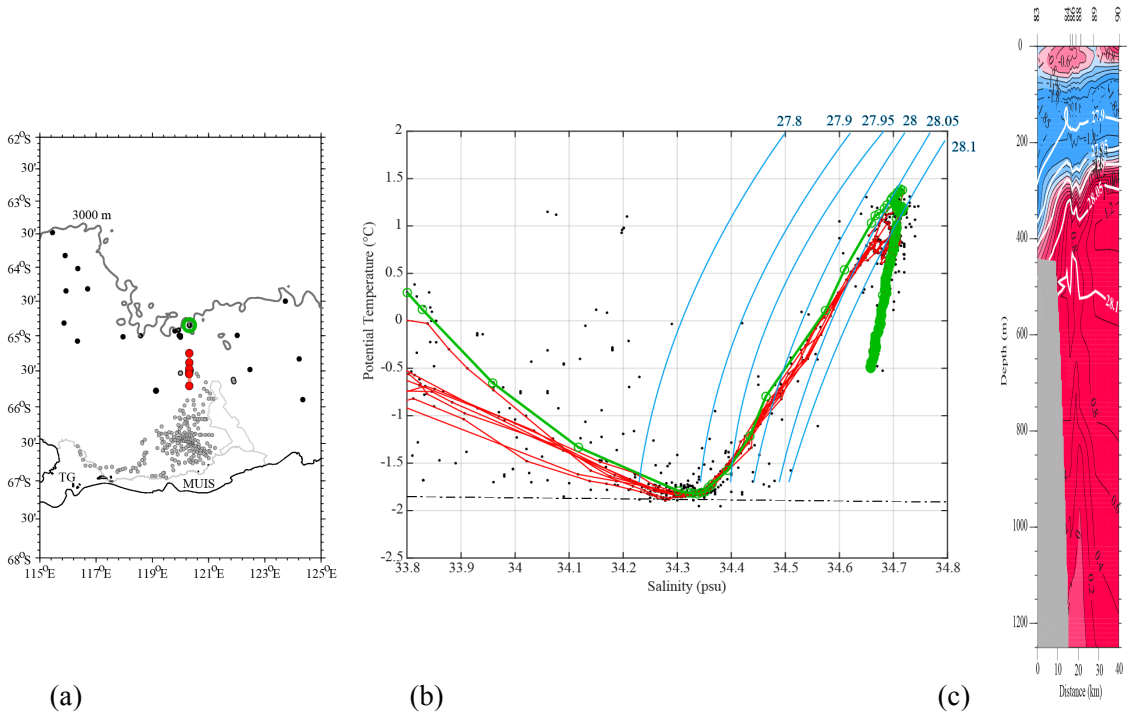


(a) (b) (c)

Figure 3. (a) Location of stations over the margins off Sabrina Coast; (b) scatter plot of their potential temperature vs. salinity, with thin cyan lines being the traces of selected neutral density surfaces; and (c) vertical distribution of potential temperature for the red stations shown in (a). Thick white contours are of selected neutral density surfaces. The green station shown in (a-b) characterizes the warmest available CDW, whereas red stations depict the cross-shelf water mass structure.

Deep expressions of the ASF are observed at the eastern Ross and Weddell Seas, where sharp poleward bends of the coastline [*Carmack & Foster*, 1975] and prevailing easterly winds [*Deacon, 1933*; *Deacon*, 1937; *Sverdrup*, 1954] facilitate the transport of AASW from near the shelf break to vast floating ice shelves along the Antarctic Coastal Current. Therefore, strong topographic steering by the massive northward-protruding Dalton Iceberg Tongue (DIT) could also channel slope waters along its western flank toward MUIS/TG.

The effective blocking of sea-ice drift from the east by the DIT promotes the development of a large ice-free area in the eastern basin off the Sabrina Coast known as the Dalton Polynya (DP; Figure 4a). Prominent and persistent coastal polynyas like the Ross Sea Polynya, the Terra Nova Bay Polynya, and the Mertz Polynya (MP; Figure 4b) are normally sustained by katabatic winds, enhanced upwelling of relatively warmer subsurface waters, and export of newly-formed sea-ice from its interior. Even though the total areal extent of coastal polynyas represents a small portion of the Antarctic shelf, they play a major climatic role by influencing regional heat and moisture fluxes, water mass transformations, gas exchange, and deep ocean ventilation *[Barber and Massom*, 2007; *Locarnini*, 1994; *Massom et al.,* 1998; *Smethie and Jacobs*, 2005; *Stössel et al.,* 2002; *Tamura et al.,* 2007; *Willmott et al.,* 2007].

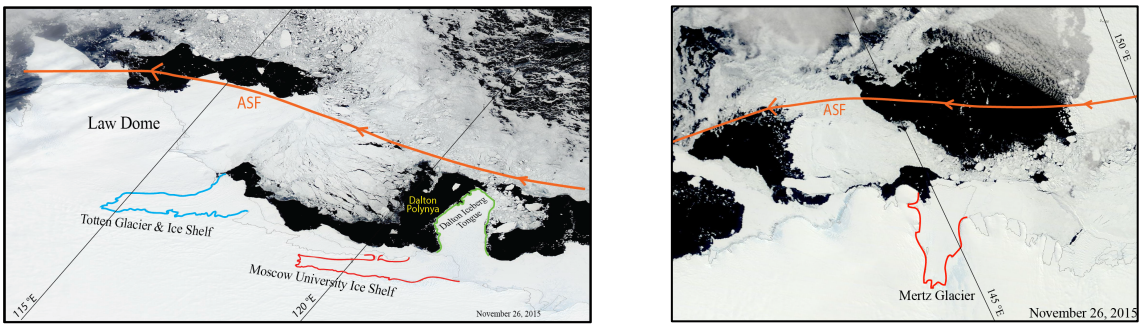


(a) (b)

Figure 4. Sea ice distribution off the (a) Sabrina and (b) Adelie coasts on 26 November, 2015 from a MODIS mosaic of visible light imagery. Solid black (white) areas indicate sea surface waters devoid of (entirely filled) sea ice.

Sea ice production within coastal polynyas, so-called "salt factories", can transform local upper waters (AASW, upwelled TW or MCDW) into much denser types of Shelf Water (SW; $\gamma^n > 28.27$ kg $m^3$). SW sinks to equilibrium levels, most of the time to the seafloor beneath polynyas and filling the deepest cross-shelf channels, as it is the densest water found over the shelf [*Whitworth et al.,* 1998]. Over shelves where SW fills the bottom layer of shelf troughs, e.g. in the western Ross and Weddell Seas, the lighter waters above are pushed upward to form a dome-like shape, which is consistent with cyclonic geostrophic circulation relative to a deeper reference level. In turn interior cyclonic cells favor intermediate inflows of TW and MCDW along the eastern limbs [*Fahrbach* 1998; *Schroder and Fahrbach*, 1999]. Progressive inshore shoaling of MDCW to near surface levels provides additional heat and salt to the southwestern sectors, e.g. in the Ross Sea where the Terra Nova Polynya opens in early spring [*Newsom, Francavillese, and Tierney*, 1965].

Source CDW available off the Adelie Coast warmer than 1.4 °C ($\theta$-max at $\gamma^n$ = 28.08 kg $m^3$, green and blue stations in Figure 5a-b) [colder than -1.7°C at $\gamma^n < 27.90$ kg $m^3$] shows identical characteristics to those off the Sabrina Coast. Its cross-ASF mixing with AASW forms MCDW ($\theta$ =0.5 °C) that progressively shoals toward the interior of the Mertz Depression. Further attenuated MCDW ($\theta$ < -1 °C) over the inner shelf lies within a thin subsurface layer, and it is transformed to denser SW through buoyancy loss (heat loss and gain in salt content) within the MP. Some SW inflows underneath the Mertz Glacier and, through basal melt, supplies outflow of Ice SW ($\theta$ < -2 °C). Cyclonic

flow of local SW to near the shelf break produces the newly-formed Antarctic Bottom Water (AABW; $\gamma^n > 28.27$ kg m$^3$) observed sinking downslope at this location.

Though inshore access of MCDW to the MUIS and TG appears limited at the eastern side of Sabrina Basin, some portion of the TW above could clear the sill and continue farther south into the central and western shelf regions off the Sabrina Coast, in particular if deep cross-shelf trenches were carved during past advances and retreats of EAIS [*Jacobs et al.,* 2011; *Jacobs and Hellmer,* 1996; *Orsi & Wiederwohl*, 2009].

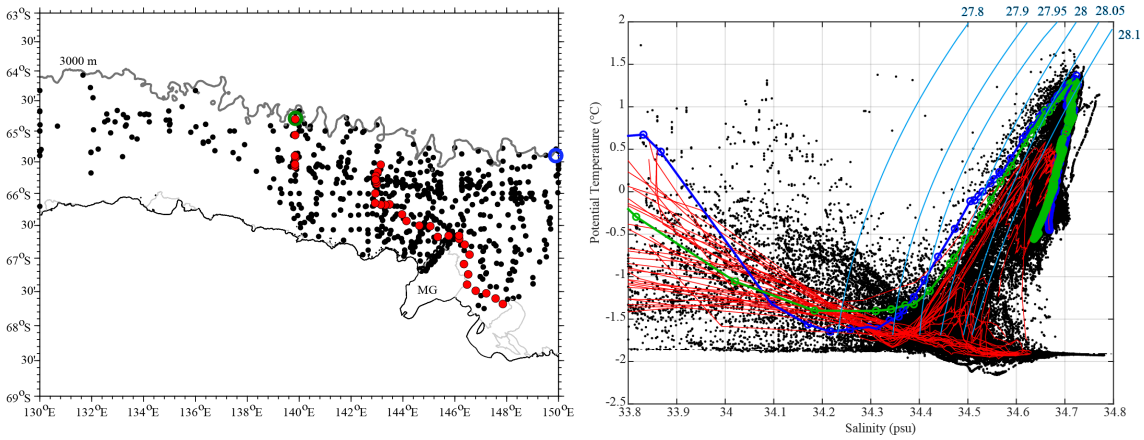


(a) (b)

Figure 5. (a) Location of stations over the margins off Adelie Coast; and (b) scatter plot of their potential temperature vs. salinity, with thin cyan lines being the traces of selected neutral density surfaces. The green and blue stations characterizes the warmest available CDW, whereas red stations depict the cross-shelf water mass structure.

## 3. NEW OBSERVATIONS OFF SABRINA COAST

As part of the U.S. Antarctic Program and funded by the National Science Foundation, a multidisciplinary scientific expedition to the continental margin off Sabrina Coast was carried out aboard the U.S. *Research Vessel Icebreaker* Nathaniel B. Palmer from January 29$^{th}$ to March 16$^{th}$, 2014 (NBP1402). A collaborative cruise funded by the Australian Antarctic Division reoccupied the area between December 5$^{th}$, 2014 and January 20$^{th}$, 2015 aboard *Research Vessel Icebreaker* Aurora Australis (AU1402). Data collected during these cruises include routine underway measurements of seafloor bathymetry, shipboard Acoustic Doppler Current Profiling (ADCP), and surface seawater temperature and salinity. Full water column profiling of physical properties consisted of stationary casts with a Seabird Niskin bottle Rosette equipped with redundant conductivity-temperature-depth (CTD) sensors, and the original use in Antarctic waters of an *Oceanscience* Underway CTD system (uCTD) with a sampling rate of 16 Hz. A summary of the data collection, reduction, quality control, and application are described in the following sections.

### 3.1. Bathymetry

Water depth was measured during NBP1402 with two hull-mounted sonars, a multibeam system and a single-ping Knudsen system. One-minute multibeam data was gridded to ~25-m resolution (Figure 6a), whereas Knudsen data from AU1402 was averaged and filtered to 1-minute intervals (Figure 6b). Due to the significant (46%) overlap of surveyed areas during both cruises, only the higher resolution multibeam data were combined to unique 1-minute Knudsen data, e.g. at the front of TG. All data were

interpolated using a nearest neighbor method to a custom, uniform 30-m longitude-latitude grid modeled after the raw multibeam resolution. The blended dataset was then objectively mapped (optimal least squares estimates) to a 600-m equal-area grid in polar stereographic projection with circular influence areas of variable radial lengths proportional to the local water. Heavy ice restricted access to the western basin, where 1-minute altimeter bathymetric data was similarly (nearest neighbor) interpolated to our adopted 600-m grid (Figure 6a-b).

Special care was taken to fill in the gaps within the adjoining band indicated by the white area surrounding the NBP1402 and AU1402 source datasets, as it was done by optimal mapping of all source bathymetric datasets using circular ellipses of influence (Figure 6-7). A map of the new blended bathymetry at a 600-m resolution is shown in Figure 7.

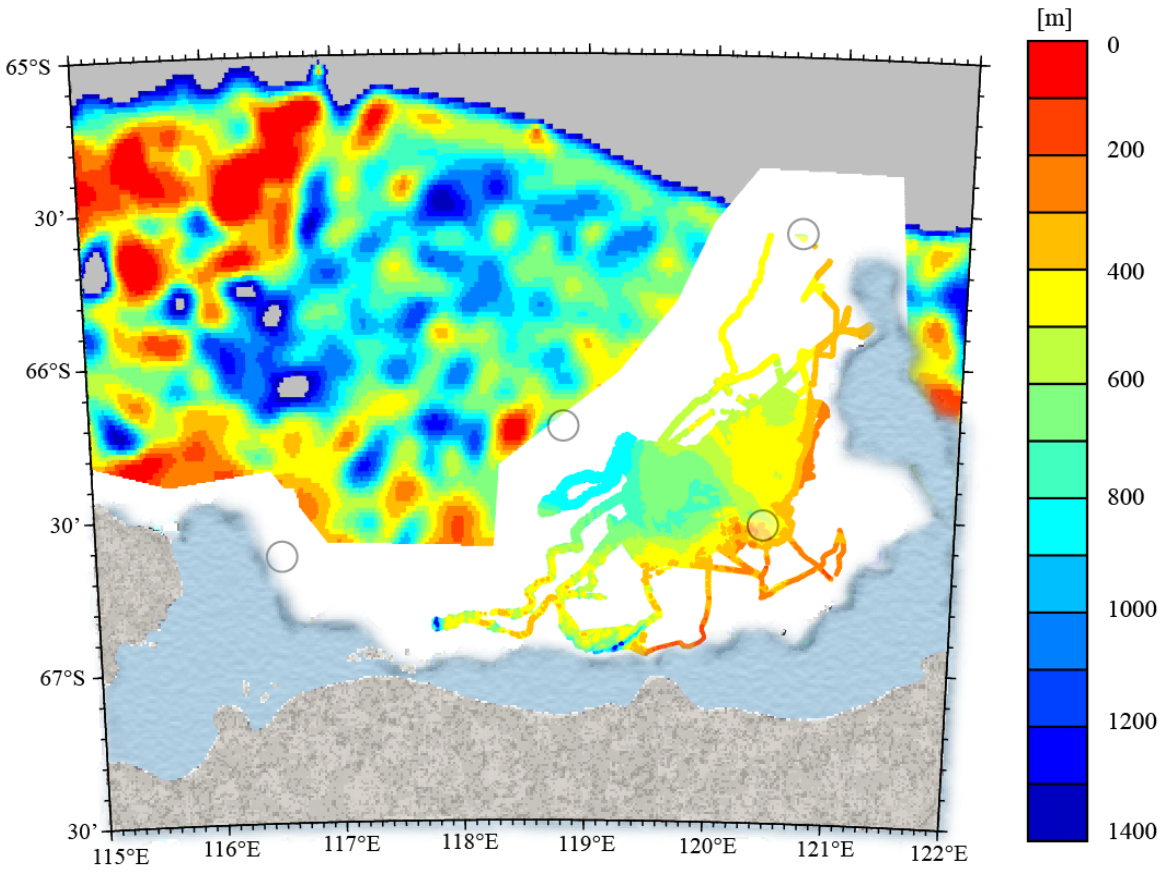


Figure 6a. Available bathymetric observations off Sabrina Coast, derived from 30-m gridded multibeam data measured during the 2014 U.S. NBP1402 cruise track (southeastern sector) and from 1-minute altimetry over the northwestern sector, with a schematic of the ellipse of influence (open circles) for optimal mapping.

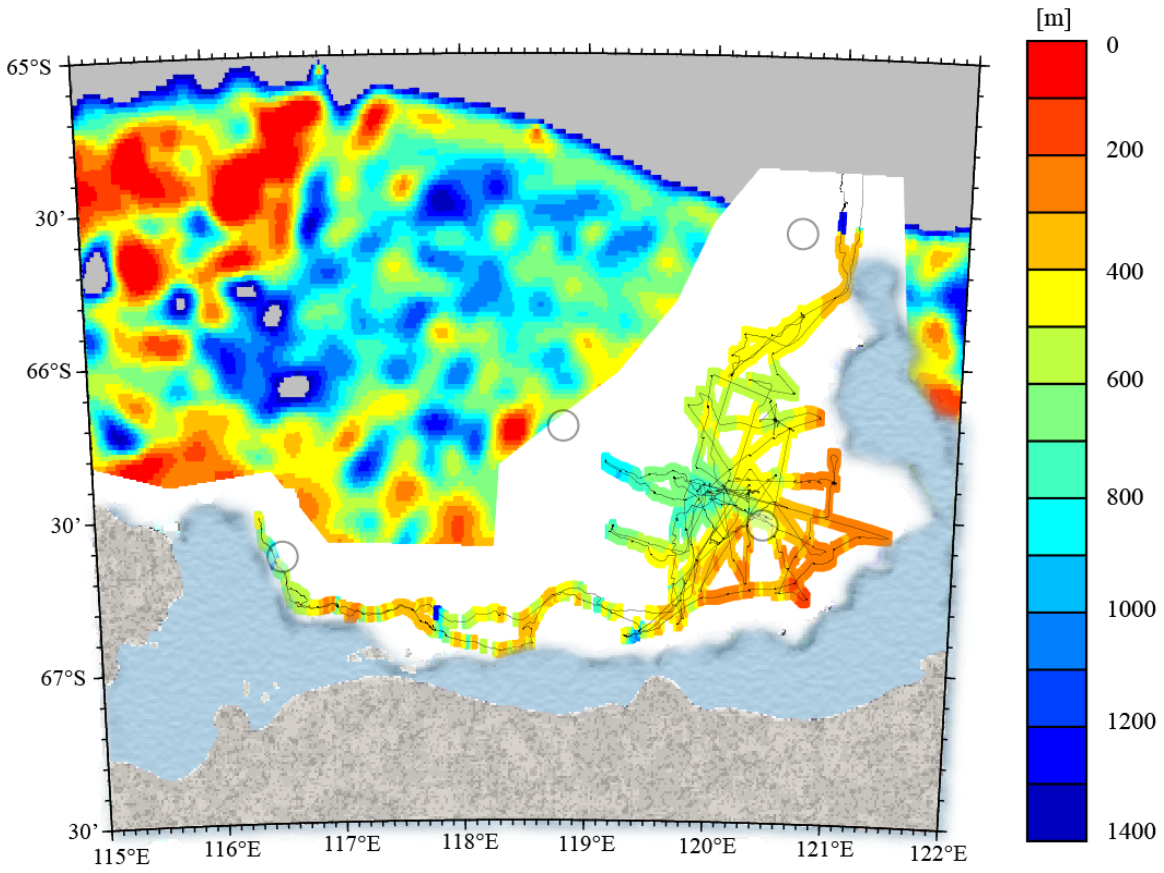


Figure 6b. Available bathymetric observations off Sabrina Coast, derived from 30-m averages of single-pin Knudsen soundings along the 2015 Australian AU1402 cruise track (southeastern sector) and from 1-minute altimetry over the northwestern sector, with a schematic of the circular ellipse of influence (open circles) for optimal mapping.

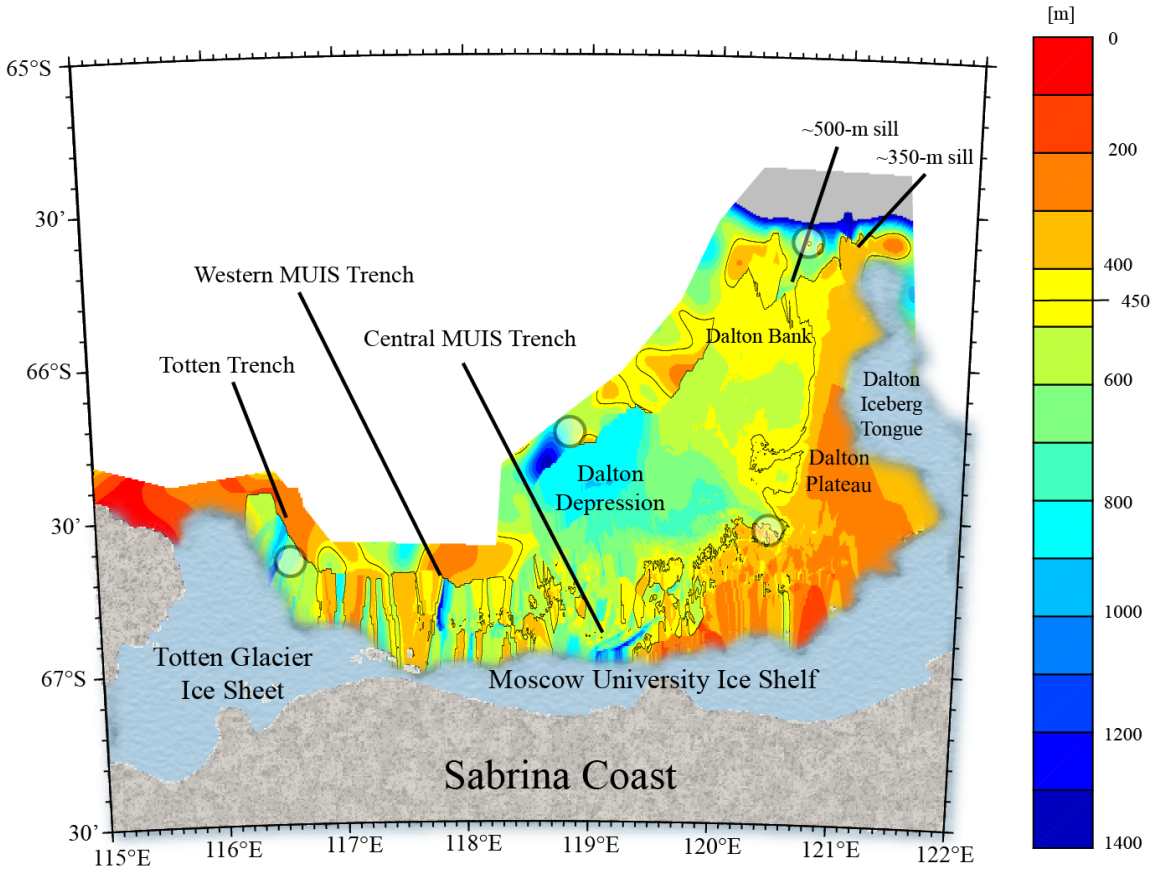


Figure 7. New bathymetric chart off Sabrina Coast derived from a gridded field with 600-m resolution using circular ellipses of influence (open circles) for optimal mapping.. Labeled place-names indicate the main topographic features, ice shelves and glaciers adopted in this study.

### 3.2. Shipboard Acoustic Doppler Current Profiling

Underway 1-min current profiling down to 1000 m was done during both cruises using Ocean Surveyor ADCPs (38 kHz, 75 kHz, 150 kHz) with maximum vertical resolution of 8 m. Initial quality control was completed using the standard Common Ocean Data Access System (CODAS) ADCP software developed at the Data Acquisition Center at University of Hawaii. This first step reduced the data set to a cleaned ADCP at 5-minute binned ensembles. More than 7000 (3500) 5-minute ensembles were preserved from NBP1402 (AU1402) (Figure 8). Tidal variability intrinsic to ADCP data was estimated using Oregon State University Tidal Prediction Software, and removed from 5-min data bins, although it proved to have an insignificant affect on the currents main direction and magnitude; thus, we conclude that tidal variability on ADCP circulation patterns derived for this region is negligible.

Antarctic data processing usually demands additional attention due to influences from the harsh environment. For example, questionable quality ADCP data is expected during slow transects through sea ice where acoustic interference becomes problematic or while stationary during science deployments. Thus, only measurements taken at ship speeds over 2 knots were further processed, which reduced the working dataset by 50%. To remove outliers from the working dataset an ad-hoc variance based filtering of ensembles located within 10 nm along the cruise track was applied, initially level-wise against two standard deviation envelopes (Figure 9) and then against entire profile standard deviations (inset of Figure 9). Individual data points falling outside these either of these envelopes were removed from our source dataset. Finally, to address data gaps

and to reduce the shear number of cleaned individual profiles (4974), a standard binning at 1.25 nm intervals along the track was applied. The spatial distribution of binned ensembles is shown by the white dots in Figure 10; the 1.25 nm spacing is ideal for combined analysis of hydrographic data, specifically for the computation of adjusted geostrophic flow at synoptic sections of CTD profiles made at average spacing of 2 nm.

Unprecedented coverage of high-resolution data resulted from underway profiling (ADCP and uCTD), and warranted the mapping of fields to the same 600-m grid used for the new bathymetry described above. All profile data were first interpolated to standard depths and to a subset of representative neutral density surfaces. The desired spatial domain was divided into seven sub-regions determined by the characteristics of the underlying seafloor topography, regional water mass properties and circulation regimes. This included the regional selection of size and orientation of ellipses of influence applied during optimal mapping, as listed in (Table 1) and portrayed in Figure 10.

| Run | Region | Offshore | East | Southeast | Southwest | Northwest | West | Hole |
|---|---|---|---|---|---|---|---|---|
| | Color | Blue | Red | Green | Magenta | Black | Cyan | Yellow |
| | Area | 51685800 | 100306 | 71022 | 57865 | 11250 | 59107 | 3029 |
| 1 | Major Axis (km) | 48.0 | 5.50 | 5.50 | 5.50 | 5.50 | 12.0 | 5.50 |
| | Minor Axis (km) | 9.60 | 12.0 | 12.0 | 5.50 | 5.50 | 5.05 | 5.50 |
| | Angle (°) | 20.0 | 0 | -40.0 | 0 | 0 | 0 | 0 |
| 2 | Major Axis (km) | 192.0 | 22.0 | 22.0 | 22.0 | 22.0 | 48.0 | 48.0 |
| | Minor Axis (km) | 38.4 | 48.0 | 48.0 | 22.0 | 22.0 | 22.0 | 22.0 |
| | Angle | 20.0 | 0 | -40.0 | 0 | 0 | 0 | 0 |

Table 1. Characteristics of adopted regional parameters for optimal mapping of property fields.

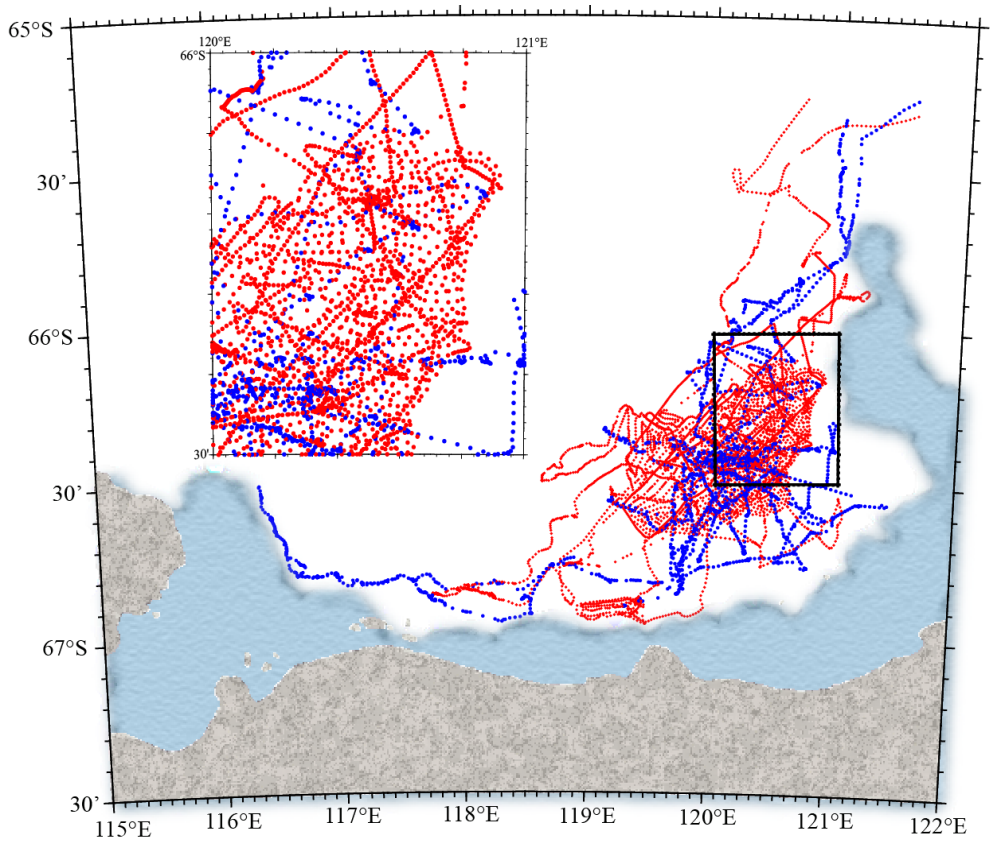


Figure 8. Spatial distribution of all available current profiling data off Sabrina Coast, corresponding to 5-minute ensembles of shipboard ADCP measurements made during the 2014 U.S. NBP1402 (red dots) and 2015 Australian AU1402 (blue dots) cruises.

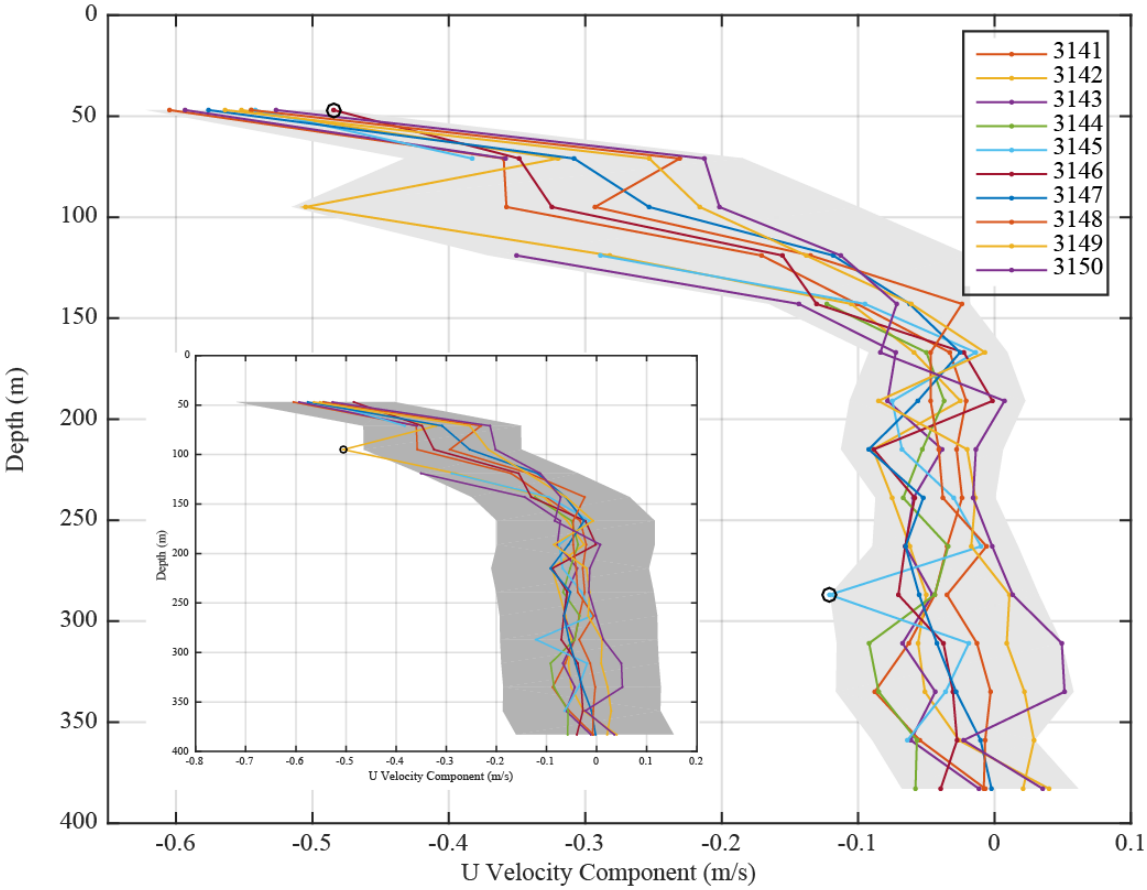


Figure 9. Example of the two-stage quality control of 5-min ADCP data. The original individual velocity profiles for the numbered ensembles are shown with color lines; and rejected data points in each stage are indicated by the black circles. The light (dark) gray shaded envelope shown in the full (inset) frame plot corresponds level-wise (full profile) ± one standard deviations calculated using ten adjacent 5-min ensembles along the cruise track.

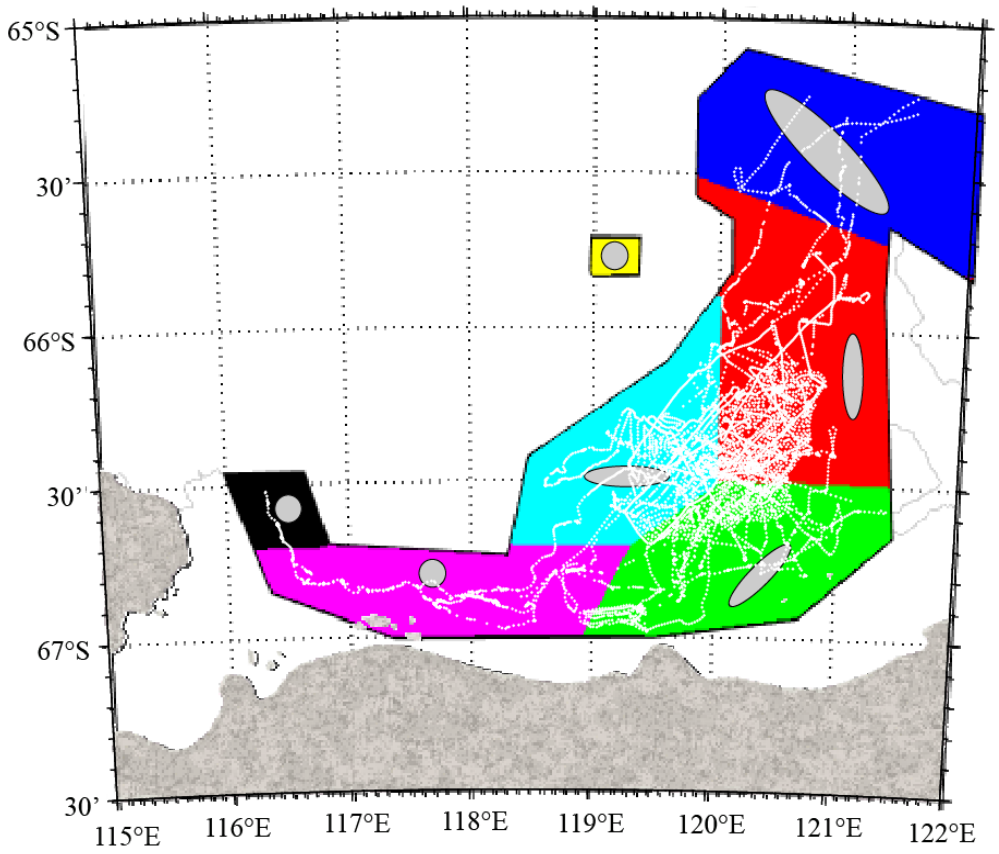


Figure 10. Adopted scheme for the optimal mapping of source ADCP data, the 1.25 nm along track averages indicated by the white dots, off Sabrina Coast. Particular lengths and orientation of ellipses of influence (gray shapes) were selected for seven sub-regions (colored polygons), as listed in Table 1.

### 3.3. Temperature and Salinity Profiling

A total of 120 and 40 underway profiles of temperature, salinity, and pressure down to 1300 m were completed during NBP1402 and AU1402. A similar number of conventional stationary CTD profiles were occupied (15 and 108 on NBP1402 and AU1402; Figure 11). After in-house quality control, a total of 123 (34) uCTD profiles from NBP1402 (AU1402) and 80 CTD profiles from AU1402 remained in the working dataset. Large offsets between duplicate CTD sensors in the rosette deployed during NBP1402 deemed data from the 15 CTD casts in that cruise unusable for the purpose of this study. In total, including BROKE and historical stations, the 232 hydrographic casts shown in Figure 11 represent the source hydrographic data in the analyses to follow.

Water mass analysis follows the classical method of comparing characteristic T-S diagrams at the station locations [*Helland-Hansen,* 1916]. Isentropic analysis of optimally mapped property fields on selected neutral density surfaces (kg $m^{-3}$) is used to describe the mixing of water masses along their spreading path [*Jackett & McDougall*, 1997; *Whitworth et al.*, 1998; *Orsi et al.*, 1999]. Additional mapping of properties at level surfaces complements the regional characterization and spatial distribution of water mass mixing and flow paths. Property and velocity vertical distributions along uCTD sections provide details on the stratification near the continental slope, across the central basin and at the Central MUIS Trench.

Profiled seawater properties, ADCP velocity, and derived neutral density and geostrophic baroclinic velocity were objectively mapped on a 3 m (horizontal) x10 m (vertical) grid along each vertical section. Baroclinic velocity profiles were individually

adjusted at each station pair with measured ADCP velocity interpolated at the corresponding reference level.

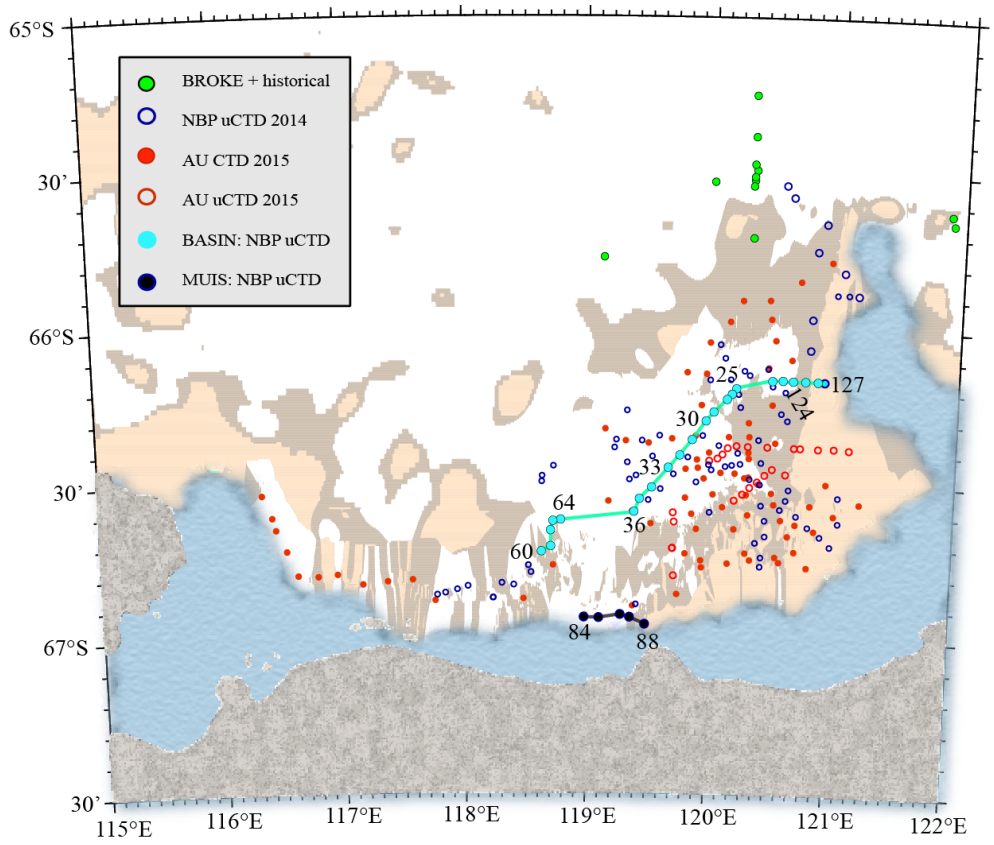


Figure 11. Location map for stations off Sabrina Coast occupied during the 2014 U.S. NBP1402 and 2015 Australian AU1402 cruises; with underway and stationary CTD profiling sites indicated with open and solid circles. Thick lines spanning numbered stations correspond to the vertical sections shown in Figures 15-16.

## 4. NEAR SURFACE CIRCULATION

The depth level with the largest number of quality controlled source ADCP data (200 m) is selected to describe the flow pattern and intensity of the near-surface circulation in the Sabrina Basin (Figure 12). The most influential topographic features (Figure 7) on the inferred circulations at 200 m are the Dalton Plateau (DPL, < 400 m) and the Dalton Bank (DB, < 500 m), with sill of about 350 m (120.8 °E, -65.6 °S) and 450 m (120.5 °E, -65.7 °S). Along the ice front a broad seafloor band, so-called basement or escarpment, is characterized by exposed bedrock with multiple deep (> 1000 m) and narrow rift fractures and trenches randomly oriented, that connect the subglacial cavities with the interior of the Dalton Depression (DD; > 600 m).

The main near surface current illustrated in Figure 12 is the nearly poleward eastern boundary current connecting DB's sill to the Central MUIS Trench (119 °E), approximately following the 450-m isobath along the western flank of DPL. An elongated anticyclonic cell is aligned with and around the top (< 300 m) of the DPL. Multiple northwestward streams are inferred at the MUIS and TG ice front, the strongest of which are located over the Central MUIS Trench. A small cyclonic cell is located over the DD. Off to the west of DIT there is a prominent northwestward outflow across the shelf break, some of which appears to return south within a tight anticyclonic cell centered at 120.6 °E and -65.75 °S.

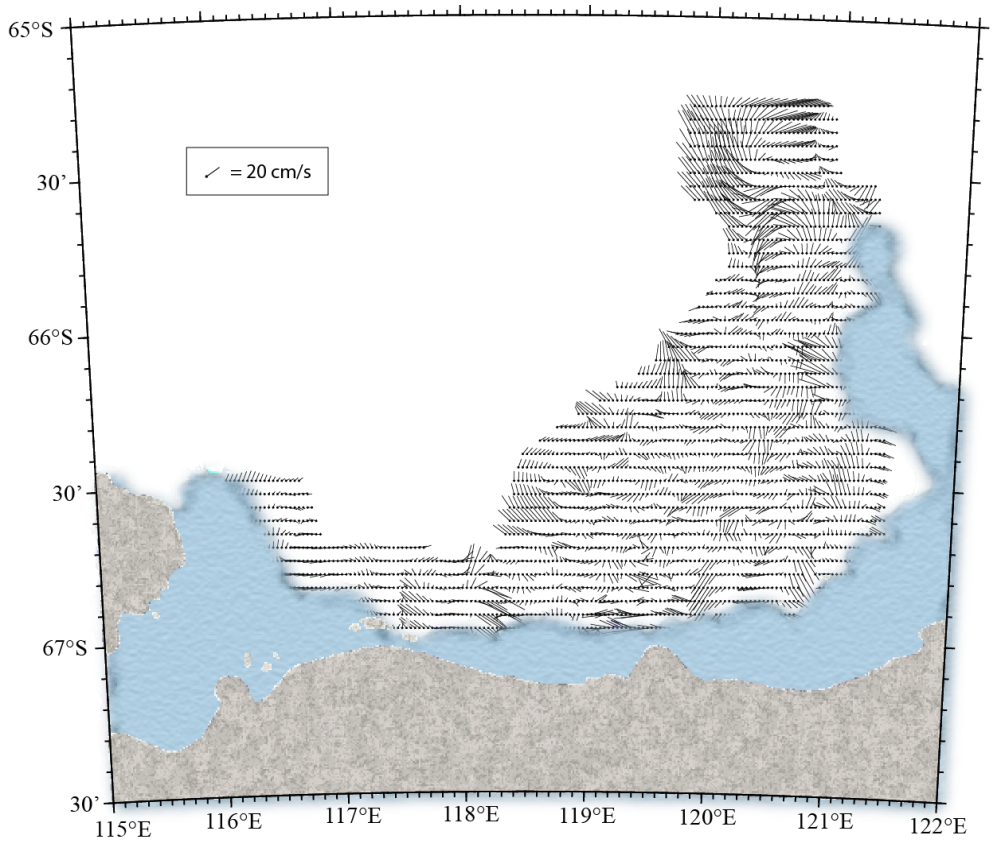


Figure 12. Map of current velocity at 200 m derived from 0.04° averages of objectively mapped ADCP data at 600-m resolution.

Next the circulation patterns at 200 m derived from direct ADCP measurements described above are compared to those inferred indirectly from the application of the geostrophic method. Assuming a deeper reference level throughout the distribution of neutral density at 200 m shown in Figure 13, cyclonic (anticyclonic) flow is indicated around centers of relatively high (low) density values, i.e. around domes (troughs) of isopycnals topography. A large cyclonic flow dominates the circulation pattern in Figure 13, with a strong eastern boundary current roughly following the 450-m isobath, in close agreement with the current's path indicated by the gridded velocity field based on direct ADCP measurements (Figure 12). Further agreement between these two independently derived maps of near surface circulation is apparent at the isolated anticyclonic cell located northwest off the DIT tip and centered at $\gamma^n < 27.80$ kg $m^3$. A similar northwestward stream is found over the Central MUIS Trench (119°E) extending into the same cyclonic cell at the DD.

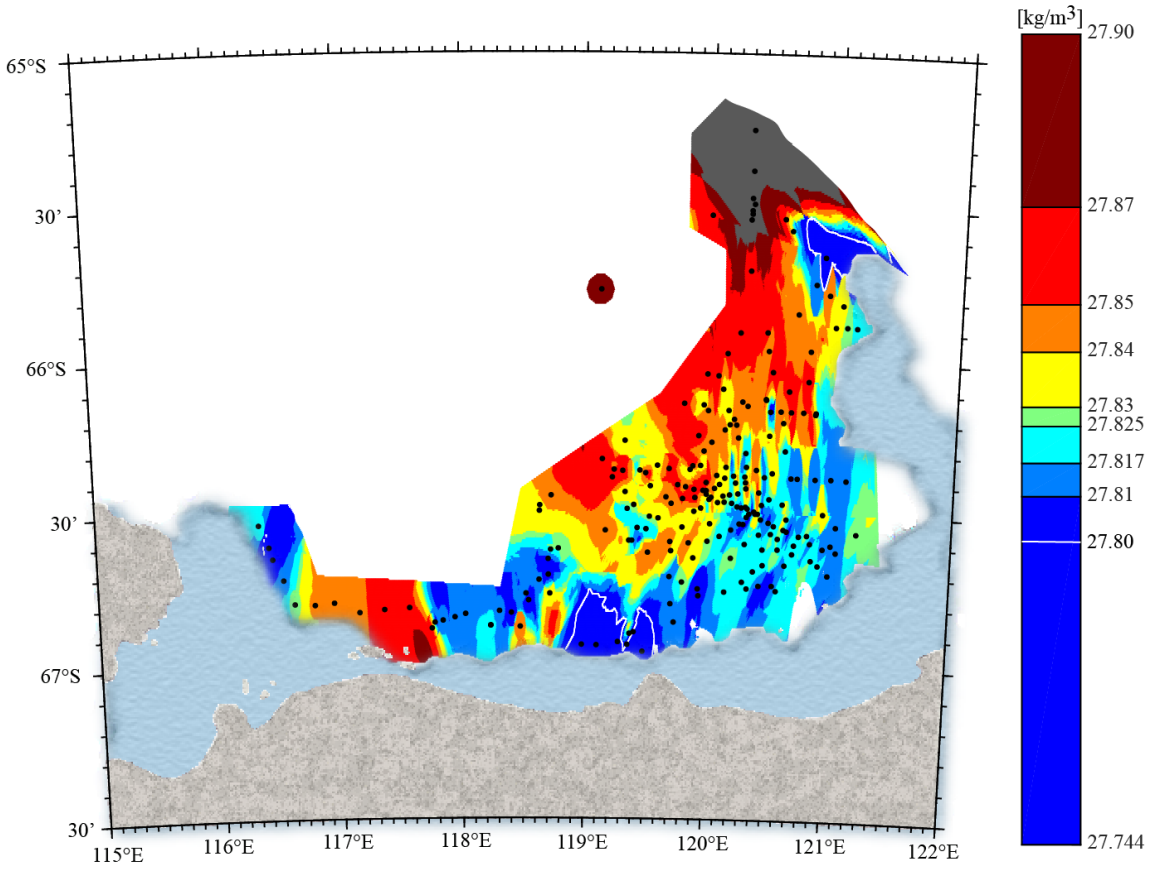


Figure 13. Neutral density at 200 m derived from CTD data objectively mapped on a 600-m grid. Black dots are the source hydrographic stations.

## 5. WATER MASS STRUCTURE AND MIXING HISTORY

### 5.1. Input and Fate of Oceanic Thermocline Water

Inspection of the T-S scatter for all NBP1402 and AU1402 CTD profiles (Figure 14) reveals a remarkable contrast between the stratifications in the Mertz and Sabrina basins, in spite of both areas having almost identical geographical and oceanographic setup. Available CDW at the slope of both regions has the same characteristics, but there is no evidence of MCDW inflows along the eastern boundary current off DIT, nor elsewhere across the eastern Sabrina Basin.

The warmest and densest input to this basin has characteristics of relatively lighter TW ($\gamma^n < 28.05$ kg m$^3$), as effectively controlled by the shelf break sills. Local MTW is found north of the sill with $\theta > 0.5$ °C (see red curves in Figure 3b), but a much attenuated signal is found within the bottom layer farther downstream as illustrated by the progression of TS curves (Figure 14) for stations at the three sections shown in Figure 12. Potential temperature, salinity and adjusted geostrophic velocity at each of the Basin and MUIS sections are shown in Figure 15a-c and Figure 16a-c. Relatively warm $\theta > 0$ °C (cyan curves in Figure 14) southward-flowing MTW is found within the bottom (350 m – 550 m) layer at the eastern (left) end of the Basin section (Figure 15a-c). However, it is not the densest portion of this MTW inflow that actively interacts with the continental ice farther to the south. The green curves in Figure 14 show that much colder MTW ($\theta \leq -1.6$ °C) fills the bottom layer of the Central MUIS Trench (Figure 16a-c). However an apparent inflection at about $\theta \sim -1.7$ °C in these stations characteristic diagrams points to source water for MUIS basal melt with $\gamma^n \sim 27.90$ kg m$^3$.

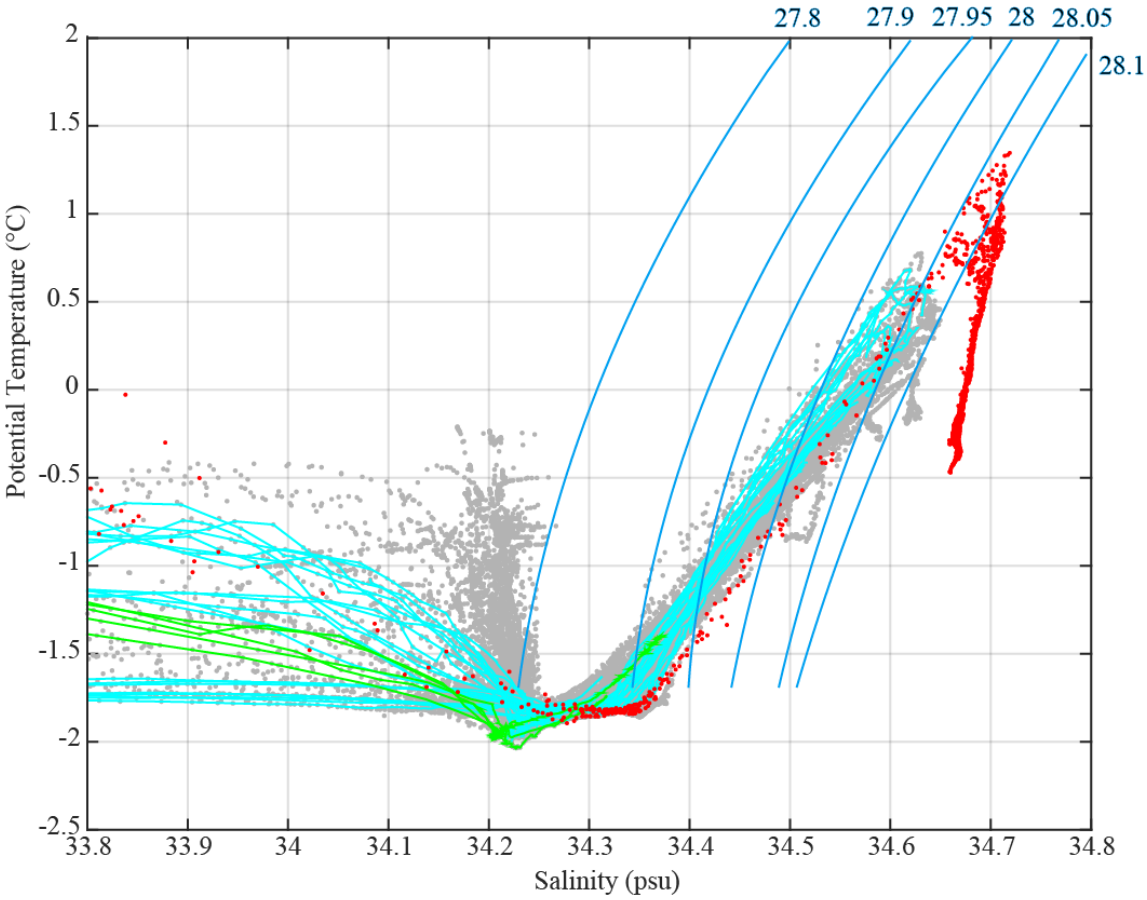


Figure 14. Scatter plot of potential temperature vs. salinity for stations off Sabrina Coast occupied during the 2014 U.S. NBP1402 and 2015 Australian AU1402 cruises. Colored curves correspond to selected profiles along each vertical section: cyan for Basin and green for MUIS. Red dots correspond to the 1996 BROKE CTD stations.

The relief of this isopycnal (Figure 17a), when interpreted with respect to a deeper reference level, portrays the geostrophic flow of MTW: shelf input of MTW happens at intermediate levels (~300 m) clearing the DB's 450-m sill; it continues directly southward along the eastern boundary current; it turns westward at the eastern end of the escarpment and thereafter it approximately follows its northern flank at ~450 m; it branches poleward descending into the Central MUIS Trench to supply the sub-glacial cavity with source water for melting at 560 m with $\theta \sim -1.7$ °C (Figure 17b); farther to the west of this trench, along the escarpment's southern boundary current, it similarly supplies the Totten Glacier Trench but with $\theta \sim -1.6$ °C at 580 m; a cyclonic interior recirculation of MTW is indicated at depths of about 320 m – 420 m within the DD, with a relatively warmer southern limb ($\theta > -1.77$ °C, Figure 17a-b).

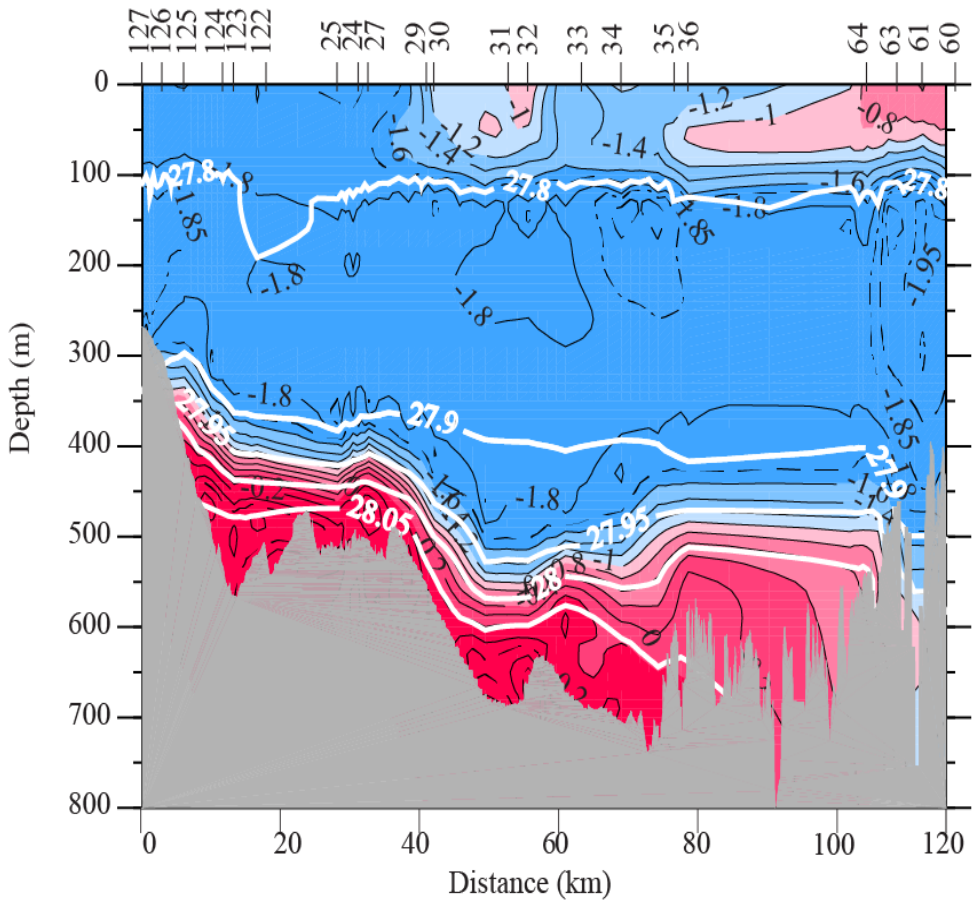


Figure 15a. Potential temperature in a vertical section across the Dalton Depression. Particular isopycnals are indicated with heavy white lines.

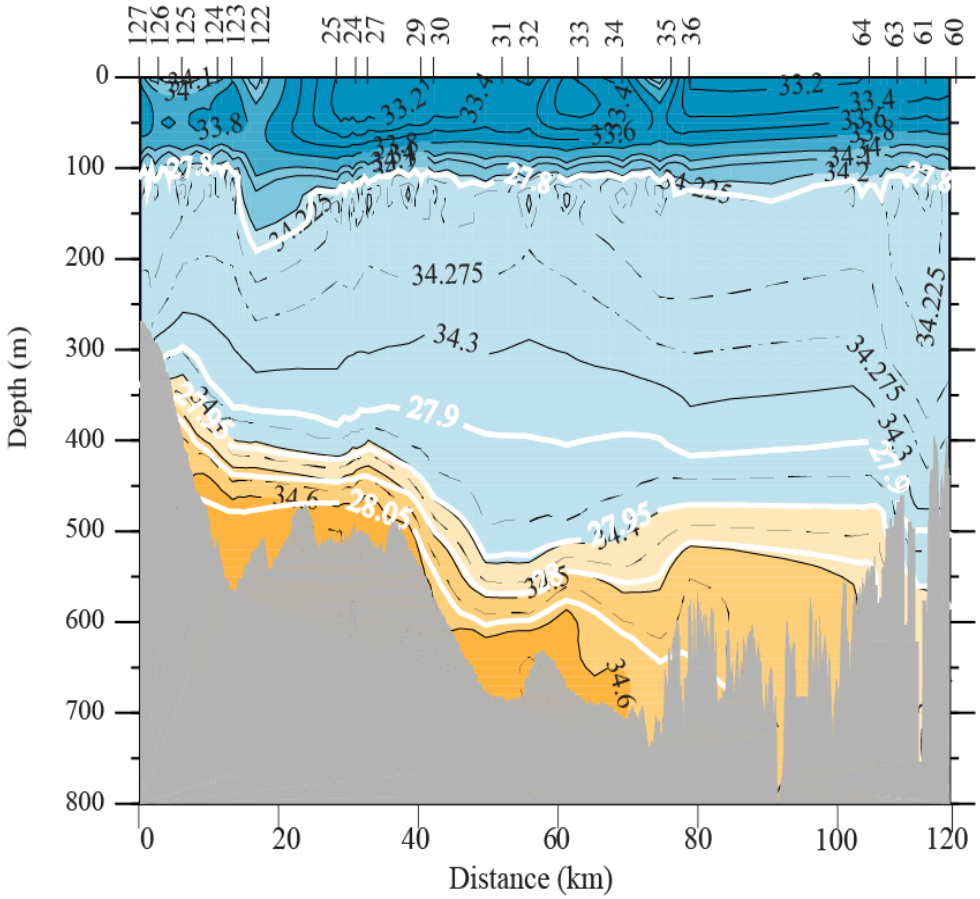


Figure 15b. Salinity in a vertical section across the Dalton Depression. Particular isopycnals are indicated with heavy white lines.

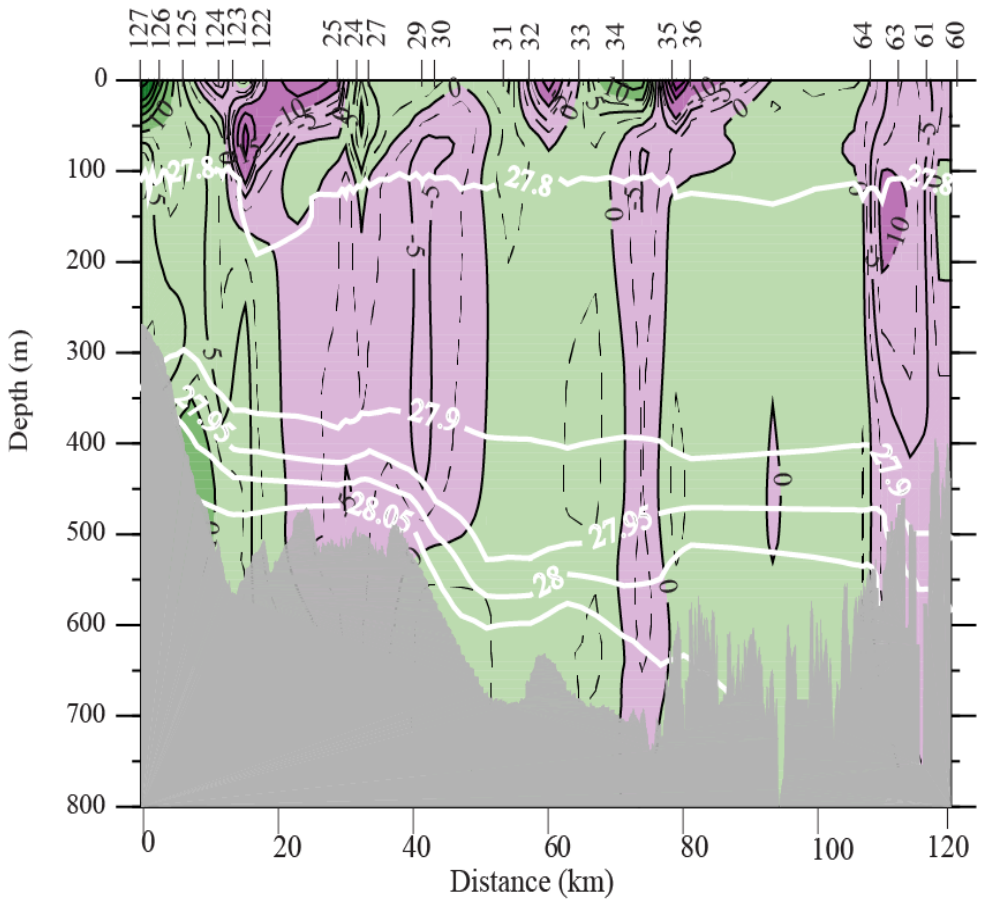


Figure 15c. Adjusted geostrophic velocity temperature in a vertical section across the Dalton Depression. Particular isopycnals are indicated with heavy white lines.

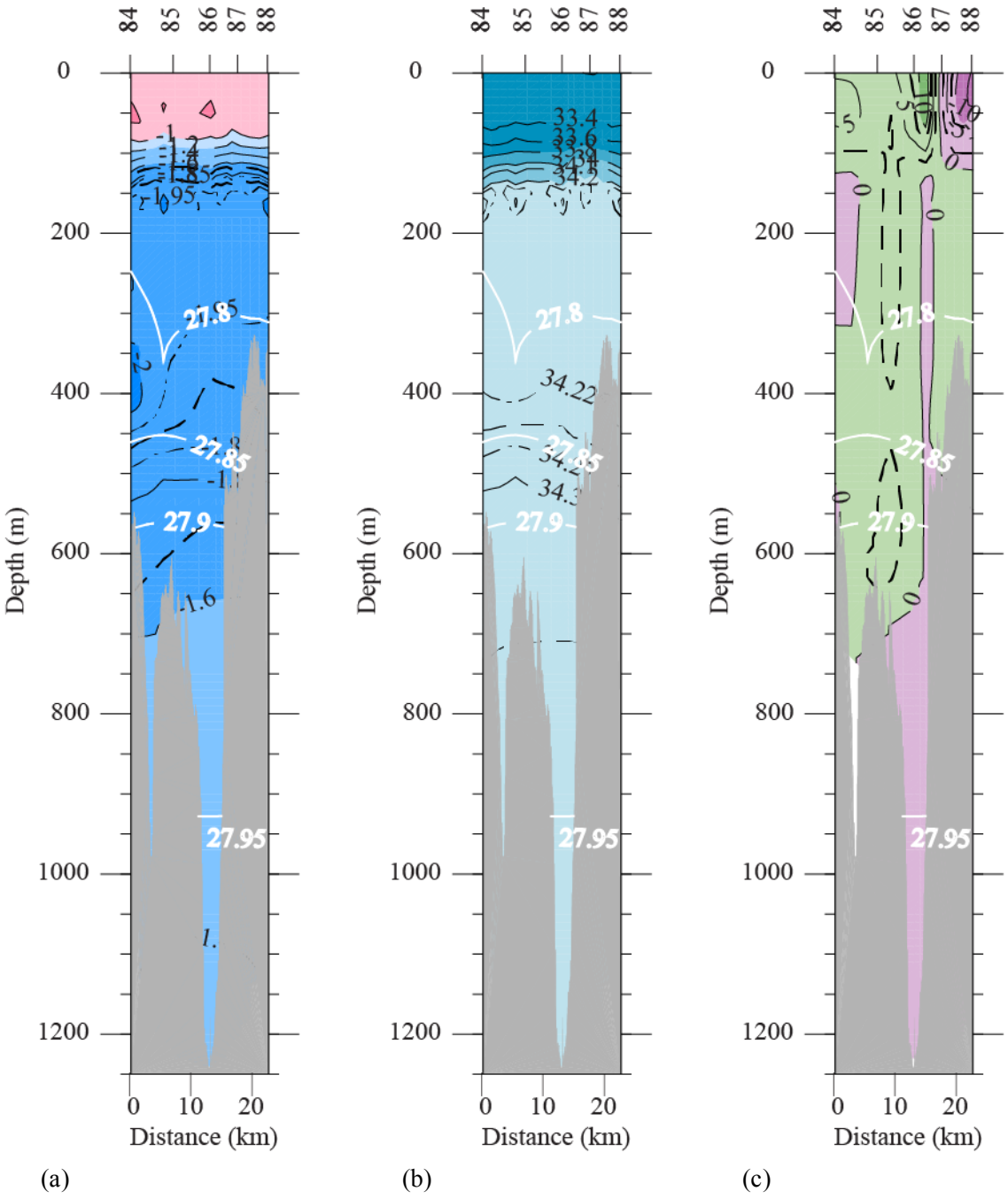


Figure 16. (a) Potential temperature in a vertical section in front of MUIS. Particular isopycnals are indicated with heavy white lines. (b) Salinity in a vertical section in front of MUIS. Particular isopycnals are indicated with heavy white lines. (c) Adjusted geostrophic velocity in a vertical section in front of MUIS. Particular isopycnals are indicated with heavy white lines.

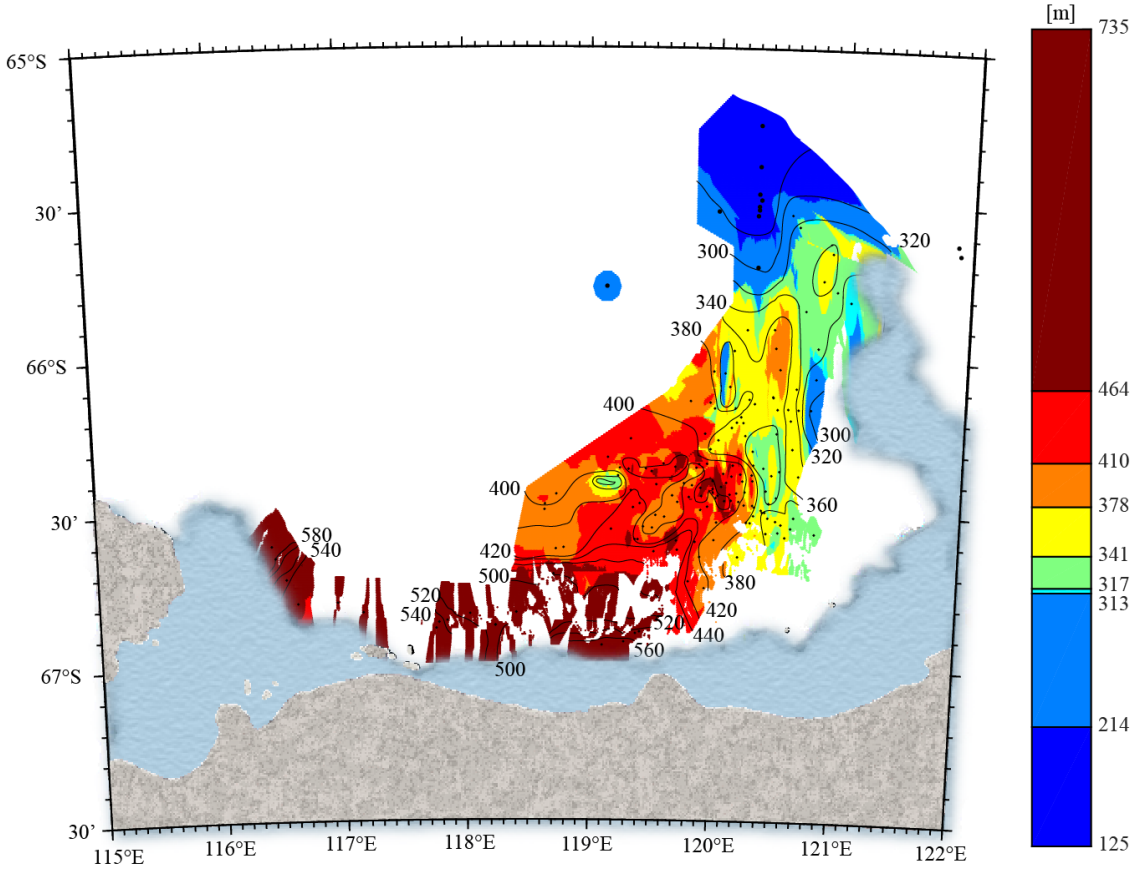


Figure 17a. Depth of the 27.90 kg $m^3$ neutral density derived from CTD data objectively mapped on a 600-m grid.

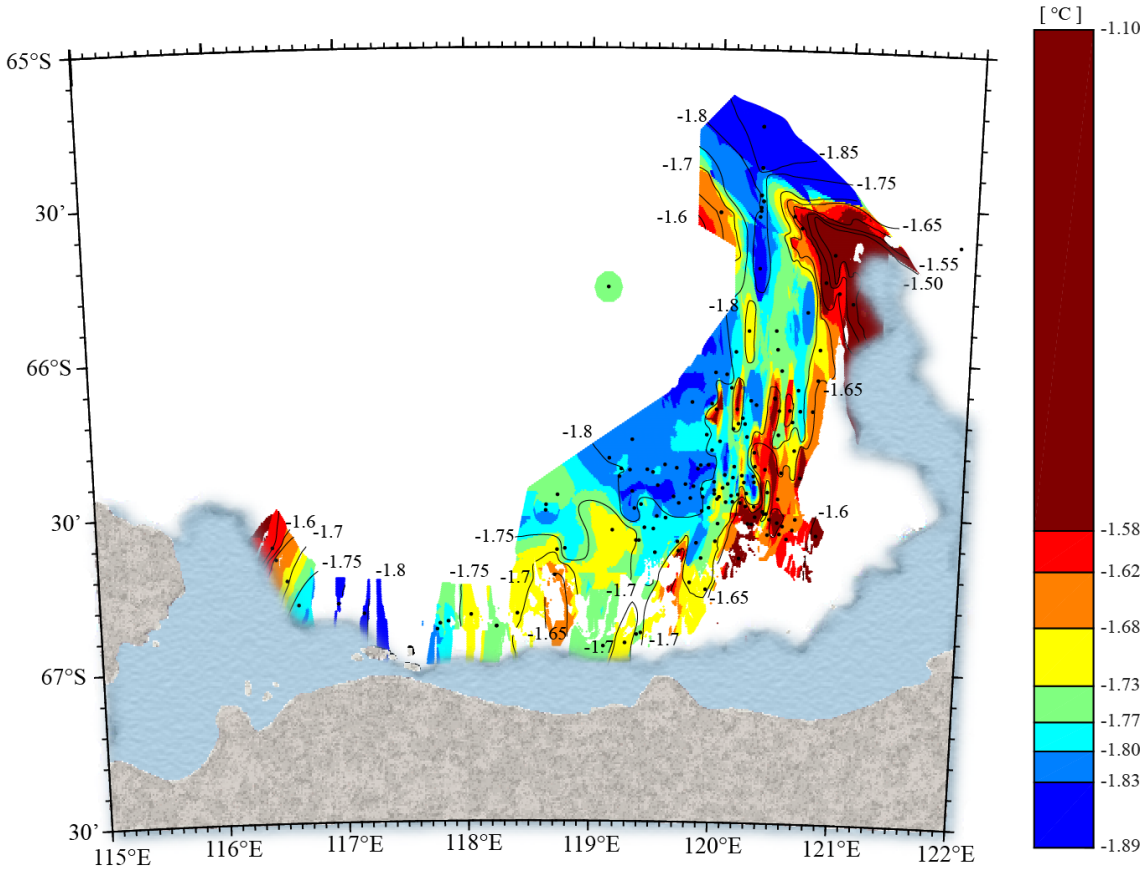


Figure 17b. Potential temperature of the 27.90 kg $m^3$ neutral density derived from CTD data objectively mapped on a 600-m grid.

### 5.2. Input and Fate of Basal Meltwater

The MUIS vertical section (Figure 16a) clearly shows a major intermediate outflow of basal MW (150 m - 450 m) within a lighter layer than the source MTW ($\gamma^n$ < 27.90 kg $m^3$) described above. It is indicated by waters with below surface freezing point potential temperatures ($\theta$ < -1.95 °C) at density levels above the MTW ($\gamma^n$ > 27.90 kg $m^3$). The downstream cyclonic circulation of this MW-bearing outflow is observed at the Basin section (Figure 15a-c), where it appears as a 300-m thick westward-flowing layer ($\theta$ < -1.85 °C) at Stas. 60-64 and its attenuated ($\theta$ < -1.8 °C) southeastward return at Stas. 32-36.

Localized buoyant plumes of MW-bearing waters are clearly indicated on property maps at 200 m (Figure 18a-b and Figure 13) at the small areas with $\gamma^n$ < 27.80 kg $m^3$ and S < 34.22, depicting northwestward injection at the Central MUIS Trench ($\theta$ > -1.95 °C) and off the tip of DIT ($\theta$ > -1.8 °C). The latter relatively warmer output is consistent with the tight anticyclonic loop inferred from the 200-m ADCP velocity distribution (Figure 11).

At 200 m, local MTW (27.90 kg < $\gamma^n$ < 28.08 kg $m^3$) available at the slope ($\theta$ > -1.7 °C and S > 34.32) turns southward across the shelf break with $\theta$ > -1.83 °C and S > 34.30 over the DB sill, and extends southeastward reaching to the DIT front near 66 °S with $\theta$ > -1.82 °C and S > 34.25. From this location, a conspicuous northward extension of anomalously warm and salty MTW ($\gamma^n$ > 27.83 kg) with origin in the oceanic domain impinges at the base of the northern DIT (65.85 °S). This is the source water for DIT

melt, whose northwestward export of MW bearing AASW ($S < 34.22$ and $\gamma^n < 27.80$ kg $m^3$) ventilated the oceanic TW while it completes the anticyclonic loop described earlier.

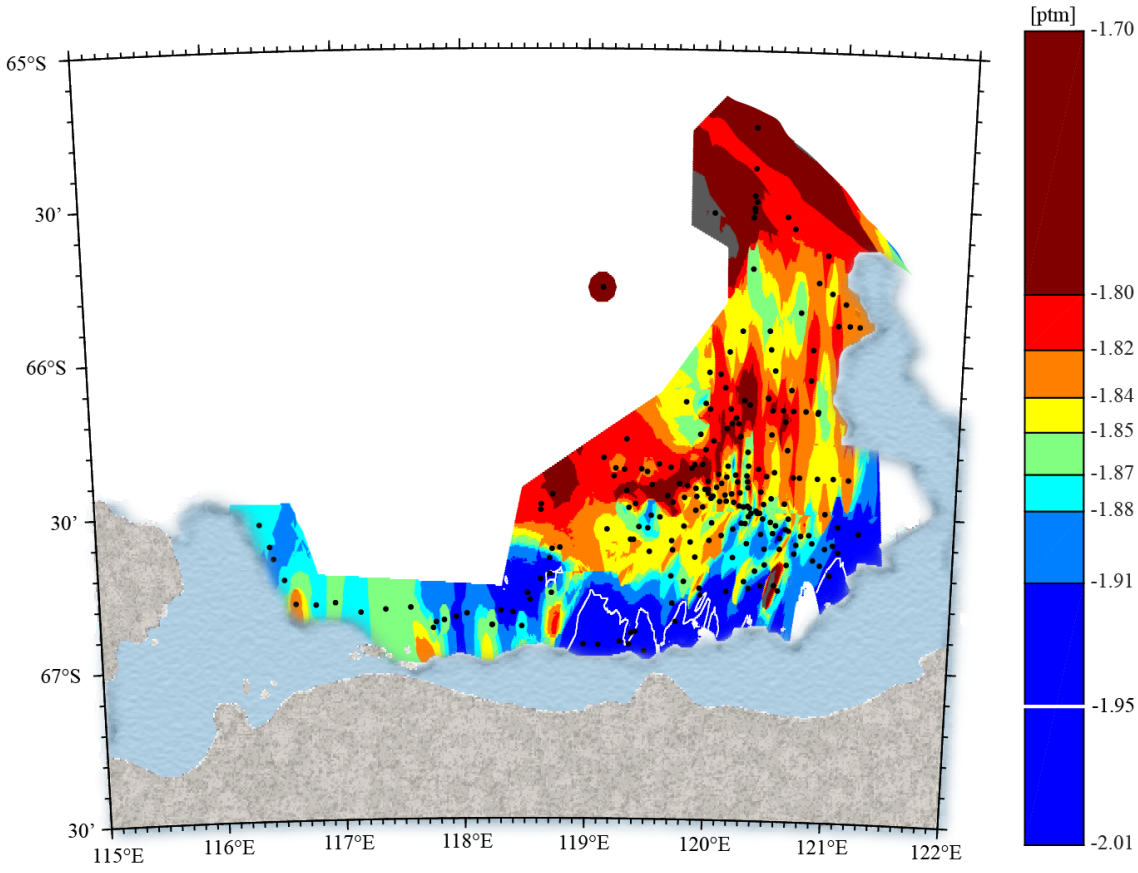


Figure 18a. Potential temperature at 200 m derived from CTD data objectively mapped on a 600-m grid.

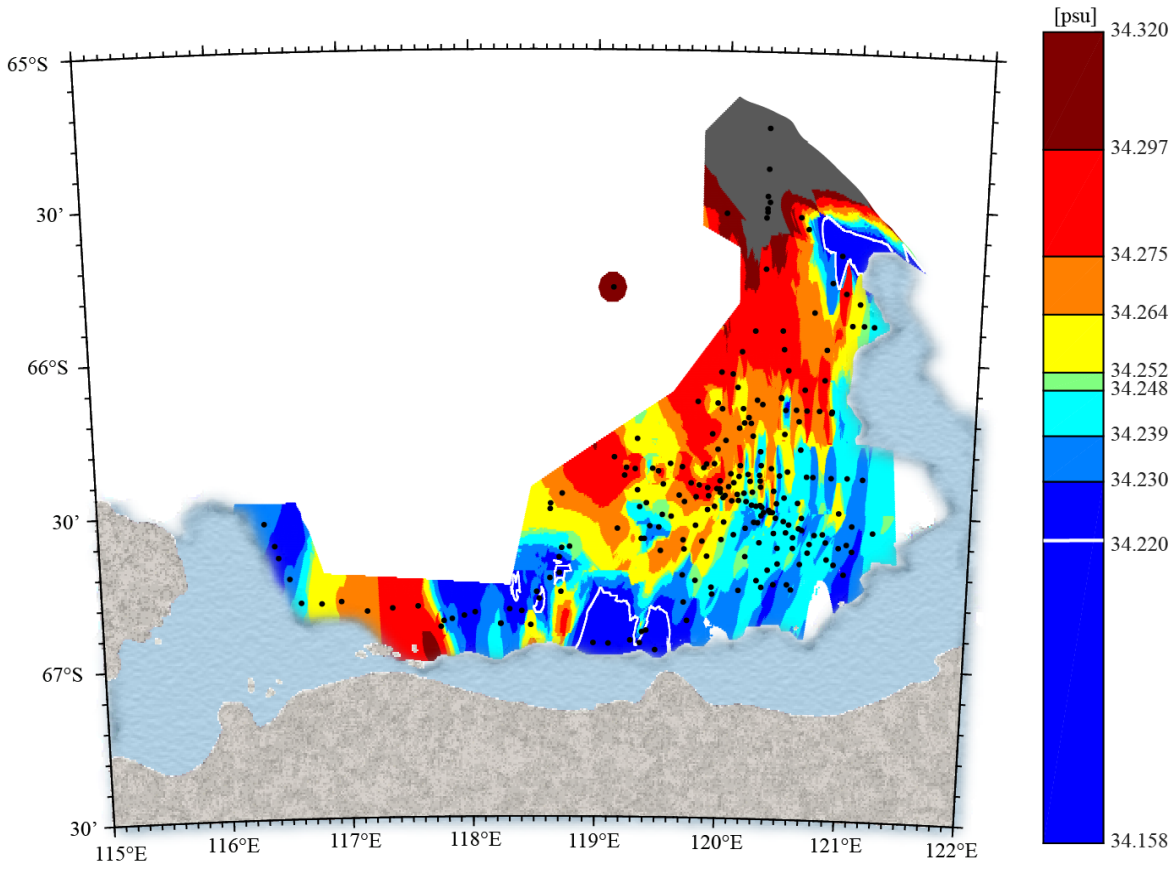


Figure 18b. Salinity at 200 m derived from CTD data objectively mapped on a 600-m grid.

# 6. SUMMARY AND CONCLUSIONS

## 6.1. Geostrophic Flow

Descriptive representations of the basin-scale time-averaged (2014-2015) baroclinic circulation of the continental margins off Sabrina Coast, East Antarctica are given by the dynamic topographies at 150/350 db, 350/500 db, and 500/600 db shown in Figure 19. The 150/350 db dynamic topography shows a general cyclonic surface circulation expressed by multiple well-developed troughs in dynamic heights of various sizes and orientation (Figure 19a). A north-south elongated cyclone along west of the DIT connects slope waters near 120 °E to the eastern end of the escarpment, and it includes a strong interior poleward boundary current extending from 66 °S to 66.5 °S.

A zonally-oriented cyclone includes a westward-flowing boundary current along the northern escarpment and its interior recirculation within the DD. Southward flow of surface water into multiple deep trenches across the escarpment are indicated at all three levels.

## 6.2. Far Fetch of Cold Thermocline Water

The available MCDW near the shelf break is blocked by the sills of the DPL (350 m) and DB (450 m). Less dense MTW is able to extend over the sills, to continue southward within a bottom temperature maximum layer along an eastern boundary current where its signal progressively attenuates and deepens: it reaches the eastern base of the escarpment ($\theta > -0.2$ °C, $\gamma^n = 28.00$ kg m$^3$) near 500 m, and sinks to the DB where it recirculates at depths greater than 500 m.

MTW with $\gamma^n = 27.90$ kg $m^3$ lying near 150 m at the shelf break is found at about 450 m over the northern escarpment, from where it descends further into the multiple trenches connected to MUIS. It supplies the source water with $\theta > -1.7$ °C lying near 560 m at the Central MUIS Trench (Figure 16, Figure 17b, Figure 19c) that supports basal melt inferred farther to the south.

### 6.3. Localized Basal MUIS Meltwater Plumes

At the Central MUIS Trench there is an intermediate export of MW-bearing AASW (Figure 19b) indicated by $\theta > -1.95$ °C and $S < 34.22$ at 200 m at $\gamma^n < 27.80$ kg $m^3$ (Figure 13, Figure 16, Figure 18). Its downstream signal is indicated by the anticyclonic flow of a thickened relatively cold ($\theta < -1.8$ °C) intermediate layer throughout the Dalton Basin (Figures 19 b-c).

Cross-slope ventilation of oceanic TW ($27.90 \text{ kg} < \gamma^n < 28.08$ kg $m^3$) is indicated along a tight anticyclonic loop west of DIT. The southeastward inflow of MTW with $\theta > -1.83$ °C and $S > 34.30$ at 200 m supplies the source water for melting at the northern DIT, from where a northwestward MW-bearing outflow is indicated by MTW with $S < 34.22$ and $\gamma^n < 27.80$ kg $m^3$ (Figure 19a, Figure 11, Figure 13, Figure 18a-b).

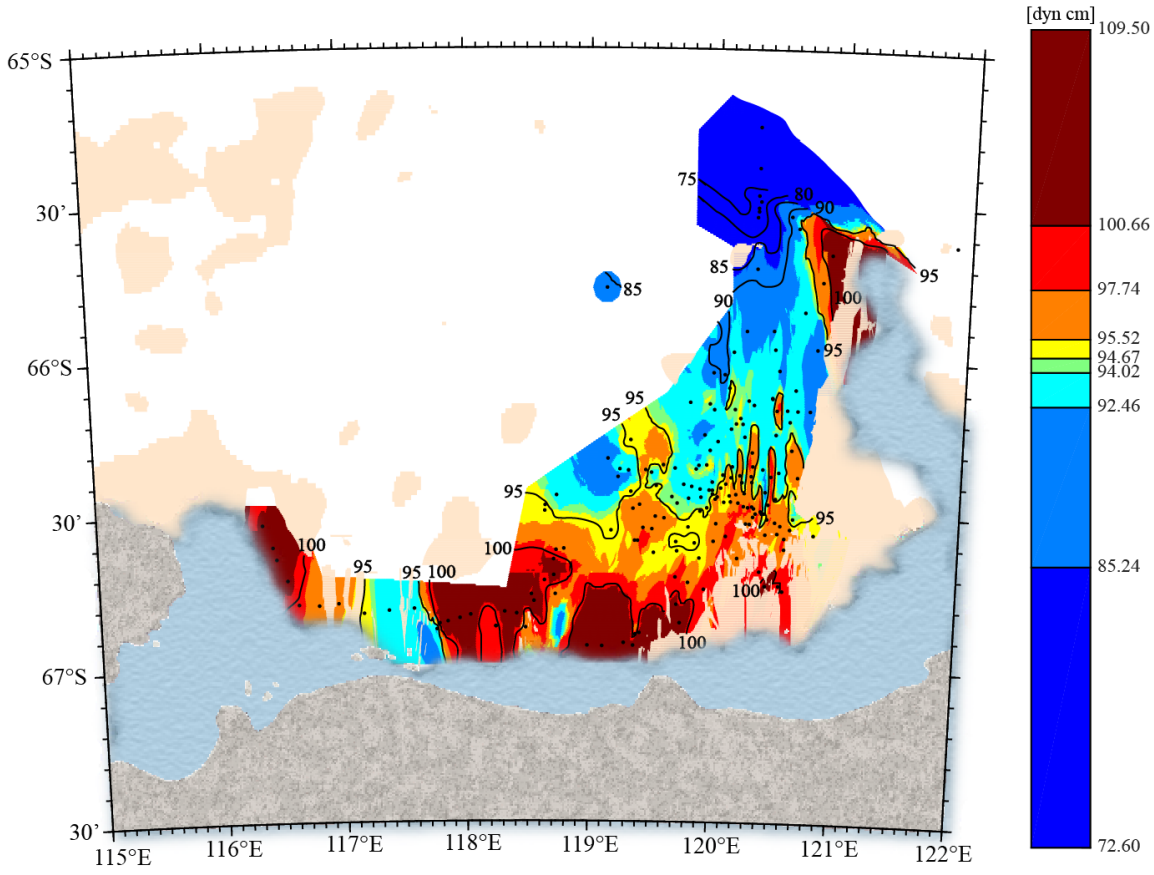


Figure 19a. Dynamic topography at 150 db relative to 350 db from objectively mapped dynamic height on a 600-m grid.

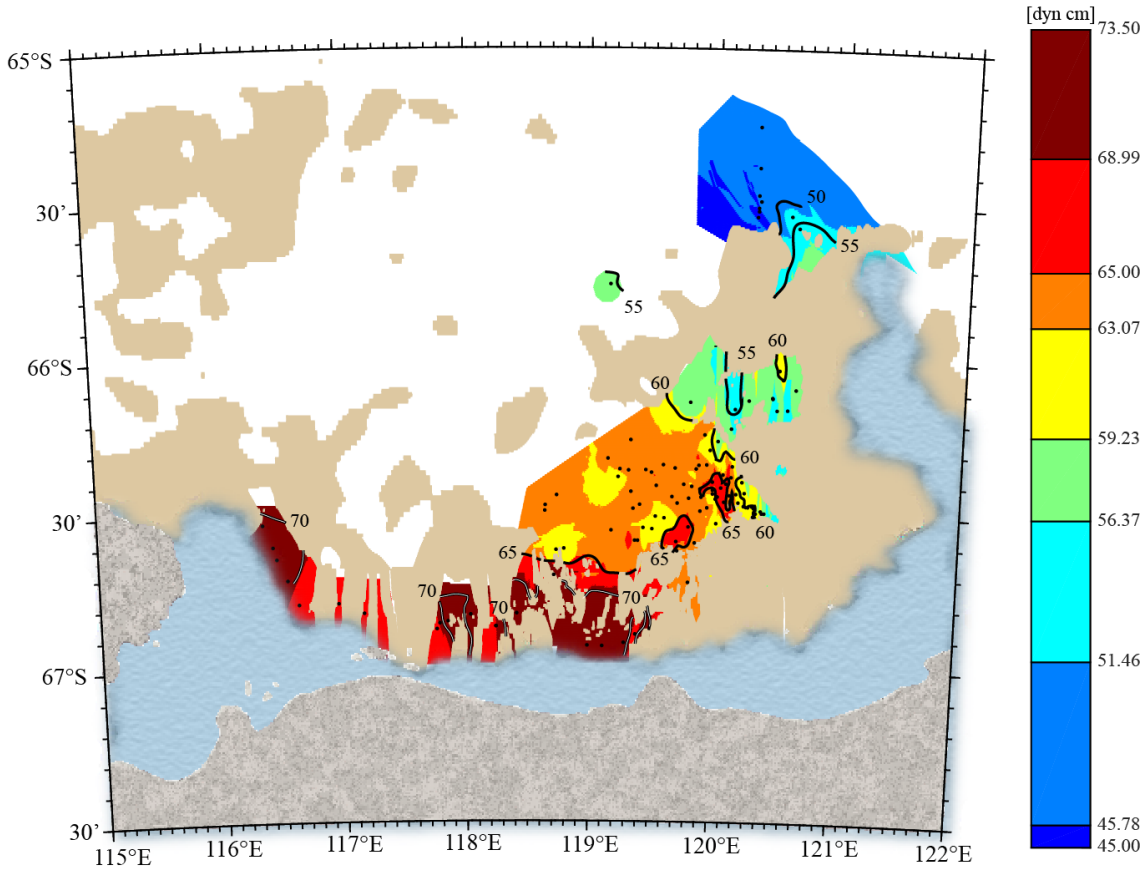


Figure 19b. Dynamic topography at 350 db relative to 500 db from objectively mapped dynamic height on a 600-m grid.

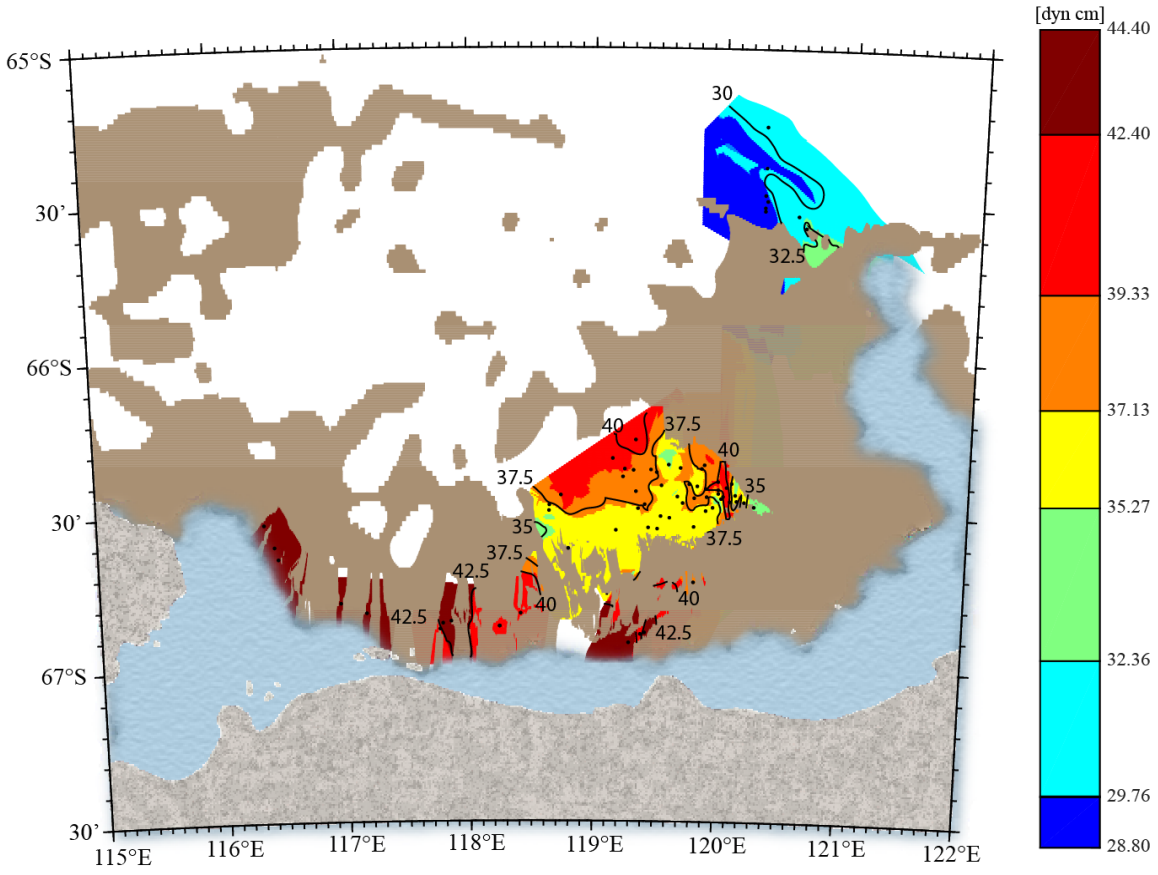


Figure 19c. Dynamic topography at 500 db relative to 600 db from objectively mapped dynamic height on a 600-m grid.

## REFERENCES

Abraham, J.P., Baringer, M., Bindoff, N.L., Boyer, T., Cheng, L.J., Church, J.A., Conroy, J.L., Domingues, C.M., Fasullo, J.T., Gilson, J., Goni, G., Good, S.A., Gorman, J.M., Gouretski, V., Ishii, M., Johnson, G.C., Kizu, S., Lyman, J.M., Macdonald, A.M., Minkowycz, W.J., Moffitt, S.E., Palmer, M.D., Piola, A.R., Reseghetti, F., Schuckmann, K., Trenberth, K.E., Velicogna, I., Willis, J.K. 2013. A Review of Global Ocean Temperature Observations: Implications for Ocean Heat Content Estimates and Climate Change. Reviews of Geophysics 51, 450-83.

Arrigo, K.R., Lowry, K.E., Van Dijken, G.L., 2012. Annual Changes in Sea Ice and Phytoplankton in Polynyas of the Amundsen Sea, Antarctica. Deep Sea Research Part II: Tropical Studies in Oceanography 71-76, 5-15.

Barber, D.G., Massom, R.A., 2007. Chapter 1 The Role of Sea Ice in Arctic and Antarctic Polynyas. Polynyas: Windows to the World. Elsevier Oceanography Series. 74.

Bindoff, N.L., Rosenberg, M.A., Warner, M.J., 2000. On the Circulation and Water Masses Over the Antarctic Continental Slope and Rise Between 80 and 150 °E. Deep-Sea Research II 47, 2299-2326.

Carmack, E.C., Foster, T.D., 1975. On the Flow of Water Out of the Weddell Sea. Deep-Sea Research 22, 711-724.

Davis, C.H., Li, Y., McConnell, J.R., Frey, M.M., Hanna, E., 2005. Snowfall Driven Growth in East Antarctic Ice Sheet Mitigates Recent Sea Level Rise. Science 308, 1898–1901.

Deacon, G.E.R., 1933. A General Account of the Hydrology of the South Atlantic Ocean. Discovery Reports 7, 171–238.

Deacon, G.E.R., 1937. The Hydrology of the Southern Ocean. Discovery Reports 15, 3-122.

Dupont, T. K., Alley, R.B., 2005. Assessment of the Importance of Ice-shelf Buttressing to Ice-sheet Flow. Geophysical Research Letters 32, 1-4.

Fahrbach, E., Klepikov, A., Schroder, M., 1998. Circulation and Water Masses in the Weddell Sea, In Physics of Ice-Covered Seas. Lecture Notes from a Summer School in Savonlinna, Finland, 6-17 June 1994, Helsinki University Press, pp. 569-603.

Fahrbach, E., Rohardt, G., Krause, G., 1992. The Antarctic Coastal Current in the Southeastern Weddell Sea. Polar Biology 12, 171-182.

Feldmann, J., Levermann, A., 2015. Interaction of Marine Ice-sheet Instabilities in Two Drainage Basins: Simple Scaling of Geometry and Transition Time. The Cryosphere 9, 631-645.

Gille, S.T., 2002. Warming of the Southern Ocean Since the 1950s. Science 295, 1275–1277.

Helland-Hansen, B., Nogen hydrografiscke metodor, Forch. Skandinaiis/'e Naturforske miite 16, 357-359, 1916.

IPCC, 2013: Climate Change 2013: The Physical Science Basis. Contribution of Working Group I to the Fifth Assessment Report of the Intergovernmental Panel on Climate Change [Stocker, T.F., D. Qin, G.-K. Plattner, M. Tignor, S.K. Allen, J. Boschung, A. Nauels, Y. Xia, V. Bex andP.M. Midgley (eds.)]. Cambridge University Press, Cambridge, United Kingdom, 1535.

Jackett, D.R., McDougall, T.J.,1995. Minimal Adjustment of Hydrographic Profiles to Achieve Static Stability. Journal of Atmospheric and Oceanic Technology 12, 381-389.

Jacobs, S.S., 1991. On the Nature and Significance of the Antarctic Slope Front. Marine Chemistry 35, 9-24.

Jacobs, S.S., Jenkins, A., Giulivi, C.F., Dutrieux, P., 2011. Stronger Ocean Circulation and Increased Melting under Pine Island Glacier Ice Shelf. Nature Geoscience 4, 519-523.

Jacobs, S.S., Hellmer, H.H., Jenkins, A., 1996. Antarctic Ice Sheet Melting in the Southeast Pacific. Geophysical Research Letters 23, 957–960.

Jenkins, A., Dutrieux, P., Jacobs, S.S., McPhail, S.D., Perrett, J.R., Webb, A.T., White, D., 2010. Observations Beneath Pine Island Glacier in West Antarctica and Implications for its Retreat, Nature Geoscience 3, 468–472.

Khazendar, A., Schodlok, M.P., Fenty, I., Lightenberg, R.M., Rignot, E., van den Broeke, M.R., 2013. Observed Thinning of Totten Glacier is Linked to Coastal Polynya Variability. Nature Communications 4, 2857.

Liu, Y., Moore, J.C., Cheng, X., Gladstone, R.M., Bassis, J.N., Liu, H., Wen, J., Hui, F., 2015. Ocean-driven Thinning Enhances Iceberg Calving and Retreat of Antarctic Ice Shelves. Proceedings of the National Academy of Science 12. 3263-3268.

Locarnini, R.A., 1994. Water Masses and Circulation in the Ross Gyre and Environs. Ph.D. Dissertation, Texas A&M University, unpublished.

Mankoff, K.D., Jacobs, S.S., Tulaczyk, S.M., Stammerjohn, S.E., 2012. The Role of Pine Island Glacier Ice Shelf Basal Channels in Deep-water Upwelling, Polynyas and Ocean Circulation in Pine Island Bay, Antarctica. Annals of Glaciology *53*, 123-128.

Massom, R., 2003. Recent Iceberg Calving Events in the Ninnis Glacier Region, East Antarctica, Antarctic Science 15, 303–313.

Massom, R.A., Harris, P.T., Michael, K.J., Potter, M.J., 1998. The Distribution and Formative Processes of Latent-heat Polynyas in East Antarctica, Annals of Glaciology 27, 420–426.

Newsom, K., Francavillese, L., Tierney, J., 1965. Oceanography in Operation Deep Freeze 62, 1961-1962. Marine Geophysical Investigations, Technical Report TR-118, US Naval Oceanographic Office, Washington, DC, 8-38.

Orsi, A.H., Whitworth III, T., Nowlin Jr., W.D., 1995. On the Meridional Extent and Fronts of the Antarctic Circumpolar Current. Deep-Sea Research Part I 42, 641-673.

Orsi, A.H., Johnson, G.C., Bullister, J.L., 1999. Circulation, Mixing, and Production of Antarctic Bottom Water. Progress in Oceanography 43, 55-109.

Orsi, A.H., Wiederwohl, C.L., 2009. A Recount of Ross Sea Waters. Deep Sea Research Part II: Topical Studies in Oceanography 56, 778-795.

Payne, A., Holland, P.R, Shepherd, A.P., Rutt, I.C., Jenkins, A., Joughin, I., 2007. Numerical Modeling of Ocean–ice Interactions Under Pine Island Bay's Ice Shelf. J. Geophysical Research 112, C10019.

Pritchard, H. D., Ligtenberg, S. R. M., Fricker, H. A., Vaughan, D. G., van den Broeke, M. R., Padman, L., 2012. Antarctic Ice-sheet Loss Driven by Basal Melting of Ice Shelves, Nature 484, 502–505.

Rignot, E., Jacobs, S., Mouginot, J., Scheuchl, B., 2013. Ice Shelf Melting Around Antarctica. Science 341, 266–270.

Rignot, E., Thomas, R. H., 2002. Mass Balance of Polar Ice Sheets. Science 297, 1502-1506.

Rignot, E., Vaughan, D.G., Schmeltz, M., Dupont, T., MacAyeal, D., 2002. Acceleration of Pine Island and Thwaites Glaciers, West Antarctica. Annals of Glaciology 34, 189–194.

Rintoul, S.R., 1998. On the Origin and Influence of Adelie Land Bottom Water. In: Jacobs, S., Weiss, R. (Eds.), Ocean, Ice, and Atmosphere: Interactions at the Antarctic Continental Margin, Antarctic Research Series 75. American Geophysical Union, Washington, pp. 151-171.

Scambos, T.A., Bohlander, J.A., Shuman, C.A., Skvarca, P., 2004. Glacier Acceleration and Thinning After Ice Shelf Collapse in the Larsen B Embayment, Antarctica. Geophysical Research Letters 31,--.

Schodlok, M. P., Menemenlis, D., Rignot, E., Studinger, M., 2012. Sensitivity of the Ice Shelf Ocean System to the Sub-ice Shelf Cavity Shape Measured by NASA IceBridge in Pine Island Glacier, West Antarctica. Annals of Glaciology 53, 156–162.

Schroder, M., Fahrbach, E., 1999. On the Structure and the Transport of the Eastern Weddell Gyre. Deep Sea Research II 46, 501-527.

Shepherd, A., Wingham, D., Rignot, E., 2004. Warm Ocean is Eroding West Antarctic Ice Sheet Geophysical Research Letters 31, L23402.

Smethie Jr., W.M., Jacobs, S.S., 2005. Circulation and Melting Under the Ross Ice Shelf: Estimates from Evolving CFC, Salinity and Temperature Fields in the Ross Sea. Deep Sea Research Part I 52, 959-978.

Stössel, A., Yang, K., Kim, S.J., 2002. On the Role of Sea Ice and Convection in a Global Ocean Model. Journal of Physical Oceanography 32, 1194-1208.

Sverdrup, H.U., 1954. The Currents Off the Coast of Queen Maud Land. Nor Geogr Tidsskr 14, 239-249.

Tamura, T., Ohshima, K.I., Enomoto, H., Tateyama, K., Muto, A., Ushio, S., Massom, R.A., 2006. Estimation of Thin Sea-ice Thickness from NOAA AVHRR Data in a Polynya of the Wilkes Land Coast, East Antarctica, Annals of Glaciology 44, 269–274.

Tamura, T., Ohshima, K.I., Nihashi, S., 2008. Mapping of Sea Ice Production for Antarctic Coastal Polynyas. Geophysical Research Letters 35, L07606.

Whitworth III, T., Orsi, A.H., Kim, S.-J., Nowlin Jr., W.D., 1998. Water Masses and Mixing Near the Antarctic Slope Front. In: Jacobs, S.S., Weiss, R.F. (Eds.), Ocean, Ice and Atmosphere: Interactions at the Antarctic Continental Margin. Antarctic Research Series 75, AGU, Washington, D.C., pp. 1-27.

Williams, G.D., Meijers, A.J.S., Poole, A., Mathio, P., Tamura, T., Kocker, A., 2011. Late Winter Oceanography Off the Sabrina and BANZARE Coast (117–128 E), East Antarctica. Deep Sea Research 58, 1194–1210.

Willmott, A.J., Holland, D.M., Morales Maqueda, M.A., 2007. Polynya Modeling. In: Smith, W.O. Jr., Barber, D.G. (Eds.), Polynyas: Windows to the World. Elsevier, Amsterdam.

Wingham, D. J., Wallis, D.W., Shepherd, A., 2009. Spatial and Temporal Evolution of Pine Island Glacier Thinning, 1995–2006, Geophysical Research Letters 36, L17501.

Worthington, L.V., 1981. The Water Masses of the World Ocean: Some Results of a Fine- scale Census. In: Warren, B.A., and Wunsch, C. (Eds.), Evolution of Physical Oceanography. MIT Press, Cambridge, pp. 42-69.

Yager, P.L., Sherrell, R.M., Stammerjohn, S.E., Alderkamp, A.-C., Schofield, O., Abrahamsen, E.P., Arrigo, K.R., Bertilsson, S., Garay, D.L., Guerrero, R., Lowry, K.E., Moksnes, P.-O., Ndungu, A.F, Post, A.F., Randall-Goodwin, E., Riemann, L., Severmann, S., Thatje, S., van Dijken, G.L., Wilson S., 2012. ASPIRE: The Amundsen Sea Polynya International Research Expedition. Oceanography 25, 40–53.